Jaime Leandro Lino Teyller

Licenciado em Ciências da Engenharia Electrotécnica e de Computadores

Contribution for the Optimization of the Design and Manufacture of Low-Resistance Short-Circuited Superconducting Coils

Dissertação para obtenção do Grau de Mestre em

Engenharia Electrotécnica e de Computadores

Orientadora: Doutora Anabela Monteiro Gonçalves Pronto,
Professor Auxiliar,
FCT, Universidade NOVA de Lisboa, Portugal

Co-orientador: Doutor João Miguel Murta Pina,
Professor Auxiliar,
FCT, Universidade NOVA de Lisboa, Portugal

Júri

Presidente: Doutor Rui Neves-Silva
Arguente: Doutor Mário Ventim Neves
Vogal: Doutora Anabela Monteiro Gonçalves Pronto

FACULDADE DE CIÊNCIAS E TECNOLOGIA
UNIVERSIDADE NOVA DE LISBOA

Setembro, 2018

Contribution for the Optimization of the Design and Manufacture of Low-Resistance Short-Circuited Superconducting Coils

Este documento foi gerado utilizando o processador (pdf)LaTeX, com base no template "novathesis" [1] desenvolvido no Dep. Informática da FCT-NOVA [2].
[1] https://github.com/joaomlourenco/novathesis [2] http://www.di.fct.unl.pt

To the memory of my Father.
To my mother and to my Aunt.
To my family and friends.

Acknowledgements

To the Department of Electrical Engineering of the Faculdade de Ciências e Tecnologia, Universidade NOVA de Lisboa, for the necessary support of this work,

To my Advisers, Professors Anabela Pronto and João Murta Pina, the warmest recognition and gratitude for all the patience, guidance, counselling and constant readiness. It really was a pleasure,

To my Professors at the Department of Electrical Engineering and other departments of the faculty along this journey, under penalty of forgetting someone. All contributed to my knowledge and here goes my special acknowledge,

To 4x4 Multitrabalhos in the person of Daniel Domingues for accepting the challenge to cut the tapes by water jet and to ITEP/KIT in the person of Drs. Wescley de Sousa and Anna Kario for cutting the tapes by the punching method,

To Professor Christopher Auretta for all the brownies and friendship that certainly sweetened this journey and Dra. Maria do Rosário Duarte for all the patience and support,

To my colleagues for the support during the course, especially to Adriana Mar, Carla Borges and Nuno Vilhena for the inputs during the present work,

To my family and friends for the constant comprehension of my absence. And especially to Luana Boavida, Nádia Marques, Dário Teca, Inalinda Fonseca, Carla Martins, Jandira Almeida, Helton Trindade, Kwame Almeida, Darcy Viera Lopes, Claudia Videira, my aunt Sofia Teyller and my mother Cristina Lino for all the support on every hour.

Abstract

The present dissertation intends to contribute to the optimization process of the design and manufacture of low-resistance short-circuited superconducting coils in an architecture developed in Department of Electrical Engineering of Faculdade de Ciências e Tecnologia (DEE-FCT) of the Universidade NOVA de Lisboa.

The design optimization of the previously proposed coil architecture is carried out in this work. After validation of the new design, the superconducting tapes are cut through two different methods, i.e. by water jet and punching. The critical current of the tapes is measured to assess the quality of the cut made and the preservation of the superconducting properties of the tapes.

The most suitable method to perform the joint of the coils is determined by measuring the contact resistance at the joints using different solder materials and configurations. Prototypes of coils with 4 and 8 turns are constructed, and an experimental test for the determination of the critical currents through the induction of superconducting currents into the coils is carried out.

It is concluded that the water jet is very aggressive to cut the tapes and difficult to adapt to large tape lengths using the current conventional machines. It is verified a better aptitude of the punching method through a cutting machine adaptable to the various moulds and lengths, conditioned by the fact that it is currently a restricted access process.

Some suggestions are made for future works which do not exhaust in this dissertation.

Keywords: High-Temperature Superconductors; Coated Conductors; Short-Circuited Coils; Low-Resistance Joints; Critical Current Density.

Resumo

A presente dissertação pretende dar um contributo ao processo de otimização inerente ao projeto e fabrico de bobinas supercondutoras em curto-circuito e baixa resistência, numa arquitetura desenvolvida no Engenharia Electrotécnica e de Computadores da Faculdade de Ciências e Tecnologia (DEE-FCT) da Universidade NOVA de Lisboa.

Realiza-se neste trabalho a otimização do design da arquitetura de bobinas anteriormente proposta. Após validação do novo design, procede-se ao corte das fitas supercondutoras através de dois métodos distintos, ou seja, por jato de água e *punching*. Determina-se a corrente crítica das fitas para aferir a qualidade do corte efetuado e a preservação das propriedades supercondutoras das fitas.

O método mais adequado à realização da junção das bobinas é determinado através da medição da resistência de contacto nas junções utilizando diferentes materiais de soldadura e configurações. Constroem-se protótipos com 4 e 8 espiras ensaiam-se experimentalmente para determinação da corrente crítica através da indução de correntes supercondutoras nas bobinas.

Conclui-se que o jato de água é bastante agressivo para o corte das fitas e de difícil adaptação para grandes comprimentos de fita utilizando as máquinas convencionais atuais. Verifica-se uma melhor aptidão do método de corte por *punching* através de uma máquina de corte adaptável aos vários moldes e comprimentos, com a ressalva de atualmente ser um processo de acesso restrito.

Efetuam-se algumas sugestões para trabalhos futuros que não se esgotam na presente dissertação.

Palavras-chave: Supercondutores de Alta Temperatura; Condutores Revestidos; Bobinas de Curto-Circuito; Junções de Baixa Resistência; Densidade de Corrente Crítica.

Contents

List of Figures

List of Tables

Acronyms

1G first generation.

2G second generation.

ABAD Alternating Beam Assisted Deposition.

Bi-2223 Bismuth-Strontium-Calcium-Copper-Oxide, $(Bi, Pb)_2Sr_2Ca_2Cu_3O_{10-x}$.

Bi-2212 Bismuth-Strontium-Calcium-Copper-Oxide, $Bi_2Sr_2CaCu_2O_{8+x}$.

BLCO Barium-Lanthanum-Copper-Oxide, BaLaCuO.

BSCCO Bismuth-Strontium-Calcium-Copper-Oxide, $(Bi, Pb)_2Sr_2Ca_{n-1}Cu_nO_{2n+4}$.

CC Coated Conductors.

DP Pancake or Double-Pancake.

EDM Electrical Discharge Machining.

EPG Electric Power Grids.

FAIR Facility for Antiproton and Ion Research.

HBCCO Mercury-Barium-Calcium-Copper-Oxide.

HTS High-Temperature Superconductors.

IBAD Ion Beam Assisted Deposition.

iSFCL Inductive Superconducting Fault Current Limiters.

ITER International Thermonuclear Experimental Reactor.

KIT Karlsruhe Institute of Technology.

LHC Large Hadron Collider.

LTS Low-Temperature Superconductors.

LW Layer-Wound.

MagLev Magnetic Levitation.

MOCVD Metal-Organic Chemical Vapour Deposition.

MOD Metal-Organic Deposition.

MRI Magnetic Resonance Imaging.

MTG Melt-Textured Growth.

NI No-Insulation.

NMR Nuclear Medical Resonance.

PCM Persistent Current Mode.

PFM Pulsed Field Magnetization.

PIT Powder-in-Tube.

PLD Pulsed Laser Deposition.

RABiTS Rolled Assisted Bi-Axially Textured Substrates.

RCE Reactive Co-Evaporation.

REBCO alloy of rare-earth elements with Barium-Copper-Oxide, RE123.

rSFCL Resistive Superconducting Fault Current Limiters.

SFCL Superconducting Fault Current Limiters.

SMES Superconducting Magnetic Energy Storages.

SQUIDs Superconducting Quantum Interference Devices.

TBCCO Thallium-Barium-Calcium-Copper-Oxide.

TSMTG Top-Seeding Melt Texture Growth.

WASP Walters Spring.

YBCO Yttrium-Barium-Copper-Oxide.

YSZ Yttrium-Stabilized Zirconia.

1 | Introduction

The present thesis addresses the design of coils made out of the second generation (2G) High-Temperature Superconductors (HTS) materials, namely from Yttrium-Barium-Copper-Oxide (YBCO) compound. Furthermore, the unavoidable points of losses introduced when considering a low-resistance non-superconducting joints approach.

These coils are intended to be used in practical applications such as Superconducting Fault Current Limiters (SFCL), and possibly in Superconducting Magnetic Energy Storages (SMES) devices and other energy systems or devices where it could fit.

1.1 Motivation

Coils and its design are fundamental for power applications, and when built from superconducting materials presents a series of advantages that can not be suppressed by conventional conductors, in spite of the great challenges that the use of these materials present due to its specific characteristics, and the cryogenic part essential for the operation in the superconducting state.

Amongst other technologies that use HTS coils, inductive SFCL which are characterised by the magnetic linkage between the primary and the secondary, require the latter to be short-circuited in order to be able to operate.

The technology underlying the SFCL projects is currently widespread, and its viability is directly related to the superconducting materials used in the process. Nevertheless, the superconducting tapes are a viable option due to its characteristics in the handling process, and with the particularity that it can now be produced in lengths of great extension and with few restrictions through processes even more mature.

There are available on the market a wide range of superconducting tapes sold in standard formats, which opens up good prospects for the optimisation of the design of low-resistance, short-circuited, superconducting coils through architectures not tested until now serving as a motto for the present dissertation. Furthermore, the HTS coils can also be used in SMES energy systems, another promising practical application.

1.2 Research Objectives

This dissertation aims to optimize aspects of the design and manufacture of short-circuited superconducting coils, in an architecture developed at the Department of Electrical Engineering of Faculdade de Ciências e Tecnologia (DEE-FCT) of the Universidade Nova de Lisboa. The specific objectives:

i. Superconducting tapes cutting and design of its geometric characteristics;

ii. Determination of the best soldering process for the joining process of the coils;

iii. Implementation and test of the prototype coils at real-scale dimensions with high number of turns.

1.3 Original Contributions

Design optimization of a low-resistance short-circuited HTS coil architecture built by commercially available 2G tape, with several numbers of turns and single joint point.

1.4 Thesis Structure

The dissertation is divided into 6 chapters.

This initial chapter, **Introduction**, summarizes the proposed work, the motivation that led to its development, the objectives to be achieved, the resulting contributions and the organization of this document.

In the second chapter, the **Literature Review** is presented bibliographical research of what exists until the present date directly related to the subject of this dissertation. Among the highlights, a brief introduction on superconductivity topic is presented, superconductors and main properties as well, HTS materials, superconducting tapes and finally coils of HTS material, the central subject of this thesis.

The third chapter, **Analysis of the Tapes Cutting Process**, describes the required steps for the prototype development from the design of the HTS coils, the cut of the tapes describing the cut methods, the determination of critical current of the tapes after the cut, ceasing with a comparison of the obtained results.

The fourth chapter, **Analysis of Joining Process**, describes the experimental procedures to join the tapes, the determination of the best join method and solder material to use.

The fifth chapter, **Development of Prototype Coils**, describes the specific parameters considered for the design of the prototype coils, present the developed prototypes, describe the experimental procedure to measure the induced currents into the prototype coils, finalizing with the presentation of the experimental results and analysis of the developed prototype coils.

The sixth and final chapter, **Conclusions and Future Work**, presents the project's conclusions, positive and negative aspects of the proposed architecture, and appoints some of the work that does not fall within the scope of the present project and for its relevance can be developed in the future.

2 | Literature Review

This chapter addresses some relevant bibliographic concepts to understand the present work. Hence, brief notions about superconducting materials, especially those of the HTS type, development and applications with particular interest for HTS coils are exposed.

2.1 Superconductors, a Brief Introduction

Demand over the years for excellent conducting materials has provided enormous technological advances and appears as one of the prominent areas of research, considering the whole set of applications that may result from it. In this context, continuous search for ideal superconductors is still an objective nowadays.

Liquefaction of gases gave an essential technique to the discovery of a new state of matter, known as the state of superconductivity. For this purpose, contributions such those made in 1823 with CO_2[1] by Michael Faraday and in 1898 with H_2 by James Dewar (also the inventor of vacuum vessel to store liquid hydrogen six years earlier), paved the way.

Later, in 1908 with liquefaction of He_2 (a noble gas with the boiling point at atmospheric pressure of 4.2 K), Heike Kamerlingh Onnes extended the available temperature range towards absolute zero (Buckel and Kleiner, 2004; Pina, 2010; Saxena, 2010). He also reported for the first time superconductivity in 1911, after his investigations of electrical properties on metals, such as the mercury in capillary tubes at helium boiling point (Kamerlingh Onnes, 1913). From his experiments three important macroscopic results describe the superconductors:

- A sudden vanishing of electrical resistance[2] on frozen mercury when approaching a temperature point of 4.2 K. This point is designated as the transition or critical temperature, T_c, and all superconductors present the same behaviour;

[1] Note that, CO_2 achieves liquid state at 217 K (above 5.1 atm, not presenting liquid form below this pressure), and H_2 has the boiling point at 20 K.

[2] According to Saxena (2010), the resistivity of a superconductor is below $10^{-27}\,\Omega$cm, which compared with an excellent conductor like copper with $10^{-9}\,\Omega$cm, can be assumed as zero resistivity (or ideal conductivity) for superconductors.

- Applying a sufficiently strong magnetic field, known as the critical magnetic field H_c, can destroy the superconducting state, even if below the T_c (Pronto, 2010; Rose-Innes and Rhoderick, 1978; Tinkham, 1996);
- There is a limit to electrical current density it can support before losing the state of superconductivity, known as the critical current density, J_c (Rose-Innes and Rhoderick, 1978). Being strongly related to the real temperature of the material and an applied magnetic field, achieving its maximum at absolute zero temperature (Pronto, 2010).

These three important results occur due to a remarkable combination of electric and magnetic properties in certain materials when cooled to extremely low temperatures, originating the state of superconductivity, according to Rose-Innes and Rhoderick (1978). Therefore, a well-defined region inside the critical surface defines the boundaries of superconductivity for a superconductor, as illustrated in Figure 2.1, whereas outside this region the material is said to be in the normal state.

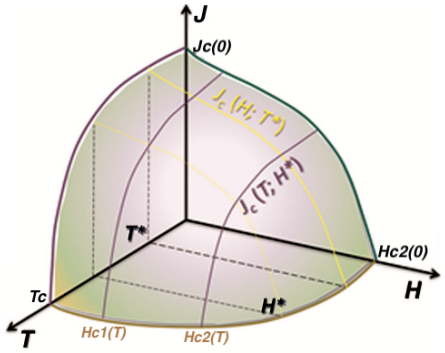

Figure 2.1: Generic phase diagram (T-J-H) of a superconductor, correlating the physical quantities described above, namely temperature, current density and magnetic field. Adapted from De Marzi et al. (2016).

Superconductors have a distinguished behaviour when in the presence of an applied magnetic field. Hence, are divided into two classes:

- Type I, characterised for being strictly associated with *Meissner effect*[3], in which, an externally applied magnetic field is expelled from within, up to a critical value of H_c, causing loss of superconductivity in the material. This class is mainly comprised of metals and metalloids of a single element[4], i.e., mercury, lead and tin (Lehndorff, 2001; Mangin and Kahn, 2017; Saxena, 2010), operating with maximum applied fields of 0.1 T, limiting the spectrum of practical applications in power energy field (De Marzi et al., 2016; Pronto, 2010).

[3] A magnetic phenomenon, known as perfect diamagnetism which shows that superconductors are not just perfect conductors, but in fact, repel the magnetic flux from within. For further notes (Pina, 2010; Pronto, 2010; Rose-Innes and Rhoderick, 1978; Tinkham, 1996).

[4] Note that, transition metals as the widely used niobium or vanadium and technetium are not of type I, but type II instead. An extended list of Type I class can be found at Eck (2018).

- Type II, formed by compounds[5] presents a more complex behaviour than type I, with two thresholds H_{c1} and H_{c2}. *Meissner effect* is exhibited till a specific value of an applied magnetic field H_{c1}, a *"mixed state"* which occurs between H_{c1} and H_{c2} values allowing the coexistence of superconducting and normal zones within the material, and the cease of superconductivity for values above the H_{c2} threshold. (Abrikosov, 2004; Buckel and Kleiner, 2004; Pina, 2010; Pronto, 2010).

  Nevertheless, near the upper critical magnetic field H_{c2}, higher flux densities are achieved, i.e., 13 T for Nb-Ti, 23 T for Nb_3Sn (Mangin and Kahn, 2017), with transition temperatures T_c above 10 K for niobium binary compounds (Lehndorff, 2001; Saxena, 2010), thus, suitable for more practical applications.

2.2 High-Temperature Superconducting Materials

Low cooling temperature of superconducting materials was an important aspect that has restrained many applications over the years, in part, due to the cost of cryogenic materials[6] and the cooling systems commercial viability. Nevertheless, a milestone was achieved in 1986 with Barium-Lanthanum-Copper-Oxide, BaLaCuO (BLCO) compound by Bednorz and Müller, presenting a transition temperature of 35 K (Bednorz and Müller, 1987). Consequently, introducing the differentiation between Low-Temperature Superconductors (LTS) and High-Temperature Superconductors (HTS), based on their required transition temperature to exhibit the superconducting properties.

The term *"High-Temperature Superconducting"* is not consensual since many authors also use to designate the superconducting materials with transition temperatures between 20 K and 50 K. However, here the term is used for the ceramic superconductors with transition temperatures above the boiling point of liquid nitrogen, i.e., 77 K at atmospheric pressure, namely, the cuprates in which layers of copper oxide alternate with other elements forming a crystallographic family known as perovskites, essentially ceramic materials.

LTS were widely used for practical applications before the discovery of HTS and are still important materials nowadays. As an example, type II binary compounds (A-15 or A_3B stoichiometry[7]) are used, presenting transition temperatures above 20 K and upper critical fields above 20 T (Buckel and Kleiner, 2004; Saxena, 2010). And compounds

[5] A list of type II superconductors constituted by alloys, binary compounds, organic compounds, cuprates (copper oxides), heavy fermions and iron-based superconductors can be found at Eck (2018).

[6] Amongst several cryogenic materials available, helium, hydrogen and nitrogen with boiling points of 4.2, 20.4 and 77.3 K respectively, are the most widespread, being liquid nitrogen the most cheaper nowadays.

[7] A stoichiometry constituted by an 'A' from the transition metals such as Nb, V, Ta or Zr and 'B' metals or semiconductors such as Sn, Al, Ga, Ge, In or Si.

as Nb-Ti and Nb_3Sn widely used for superconducting magnets construction, takes advantage of the higher upper critical field characteristic of the type II superconductors, presenting current densities above 10^9 Am^{-2}, i.e., hundred times higher than those obtained in copper wires (10^7 Am^{-2}) (De Marzi et al., 2016).

HTS discovery provided an all-new set of superconducting materials, although, the most used are based on yttrium variants of YBCO and Bismuth-Strontium-Calcium-Copper-Oxide, $(Bi, Pb)_2Sr_2Ca_{n-1}Cu_nO_{2n+4}$ (BSCCO)[8]. Table 2.1 shows some cuprates that present higher transition temperatures (some at high pressures such as mercury Hg1223 at 16 GPa[9]), and highlight the extreme anisotropy of these compounds showing the upper critical density fluxes for different applied magnetic fields according to the planes orientation (perpendicular or parallel to the CuO_2 layers).

Table 2.1: Characteristic data of some cuprate superconductors with higher transition temperatures and upper critical fields (higher at low temperatures in some cases, e.g., at Tc = 0 K as reported by Sekitani et al., 2004 for an optimally doped YBCO and in Barth, 2013). Table data are taken from Buckel and Kleiner (2004).

Designation	**Composition**	$\mathbf{T_{c,max}}$ **[K]**	$\mathbf{B_{c2\perp CuO_2}}$ **[T]**	$\mathbf{B_{c2//CuO_2}}$ **[T]**
YBCO or Y123	$YBa_2Cu_3O_{7-x}$	93	110	240
BSCCO or Bi2212	$Bi_2Sr_2CaCu_2O_{8+x}$	94	>60	>250
BSCCO or Bi2223	$Bi_2Sr_2Ca_2Cu_3O_{10+x}$	107	40	>250
TBCCO or Tl2212	$Tl_2Ba_2CaCu_2O_{8+x}$	97	27	120
TBCCO or Tl2223	$Tl_2Ba_2Ca_2Cu_3O_{10+x}$	125	28	200
HBCCO or Hg1212	$HgBa_2CaCu_2O_{6+x}$	127	113	450
HBCCO or Hg1223	$HgBa_2Ca_2Cu_3O_{8+x}$	135	108	–
HBCCO or Hg1234	$HgBa_2Ca_3Cu_4O_{10+x}$	125	100	>200

Nowadays superconductivity represents a broader phenomenon as seen in section 2.1 and can be found on many metallic[10] elements of the periodic table, as, on many alloys, binary and ternary compounds, organic superconductors and lately discovered HTS. A timeline with some of the more relevant superconductors found after the discovery of superconductivity phenomenon is represented in Figure 2.2 along with its maximum transition temperatures, T_c, and reference cryogenic materials used to cool them.

Research on different types of superconductors continues with prolific achievements, improving the already known and synthesizing new ones. In this thesis, the focus is pointed to those with the increased T_c known as HTS, due to economic viability and reduced cooling costs with liquid nitrogen, for power applications.

[8] BSCCO here with a generic composition of $(Bi, Pb)_2Sr_2Ca_{n-1}Cu_nO_{2n+4}$ is presented in two varieties (n = 2 or 3).

[9] Note that, 1 GPa (giga-Pascal) = 10000 bar or 10 kbar.

[10] Note that, the most conductive ones like gold, silver and copper are excluded since their lattice does not provide the necessary conditions for the occurrence of superconductivity (Eck, 2018; Pina, 2010)

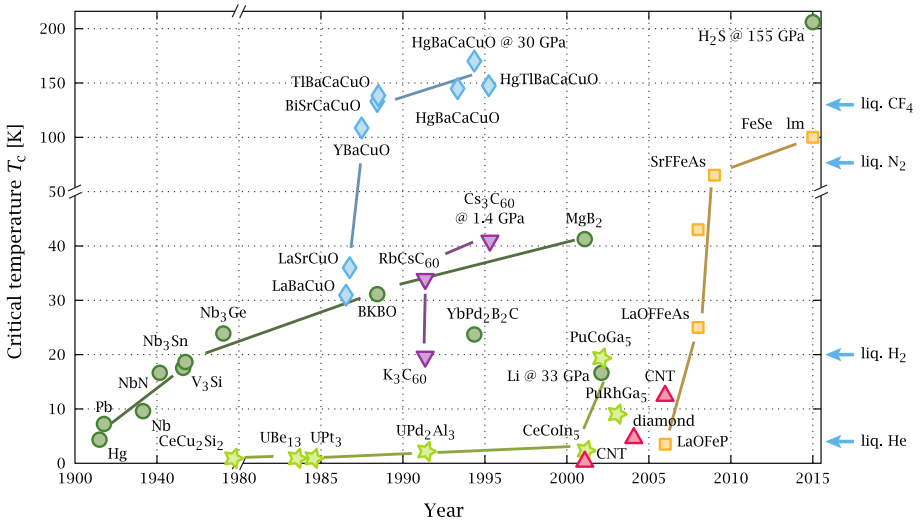

Figure 2.2: Timeline of some known superconductors. Special note for the cuprates (blue diamonds) where the BSCCO and YBCO are inserted). Taken from Jensen Ray (2015).

2.2.1 Available Commercial Forms

HTS materials commercially available in the market and considered for technological applications are predominantly YBCO and BSCCO variants, under bulk, wire and tapes.

- ***Bulk Materials***

Bulks made out of YBCO are the main available form with two different structures. Monocrystalline with higher current densities or the polycrystalline with strong anisotropy, in which, the current is limited by high-angle grain boundaries that increase barriers to the current flow, acting as weak links (Krabbes et al., 2006; Pina, 2010; Seidel, 2015). Figure 2.3 shows a bulk material with YBCO composition available in the market.

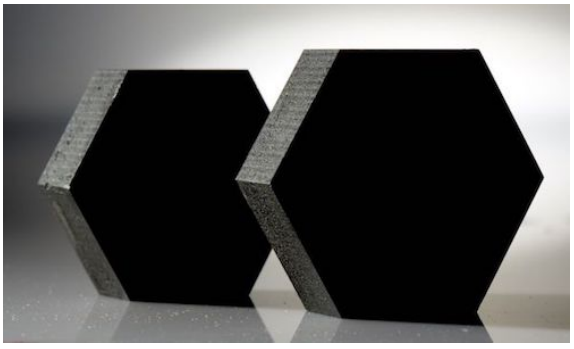

Figure 2.3: Seeded melt growth bulk from YBCO supplied as levitation disks with $T_c \sim 90$ K and trap magnetic field up to 1.4 T. Taken from Can Superconductors s.r.o. (2018).

Materials in this form are obtained by Melt-Textured Growth (MTG) processes, especially by modified techniques as Top-Seeding Melt Texture Growth (TSMTG), which permit the manufacture of single or multiple grain superconductors (Krabbes et al., 2006;

Lehndorff, 2001). In this technique, an alloy of rare-earth elements with Barium-Copper-Oxide, RE123 (REBCO) crystals as Sm123 or Nd123, with a higher melting temperature than Y123 are put on top of the precursor YBCO compacted pellet, serving as nucleation centres where crystallization starts and subjected to annealing treatment cycles to build the bulk.

- ***Superconducting Wires***

HTS wires are essentially made of BSCCO material, and the Bismuth-Strontium-Calcium-Copper-Oxide, $Bi_2Sr_2CaCu_2O_{8+x}$ (Bi-2212) variant is used to build round-wires and multifilamentary strands, using the knowledge gained on LTS wires and cables (De Marzi et al., 2016; Senatore et al., 2014).

Bi-2212 is very brittle, therefore, is subjected to Powder-in-Tube (PIT) techniques as shown in schematic of Figure 2.4, and to heat treatment processes with the diffusion of oxygen into HTS composites to form the conductors which are then filled into sheaths of silver alloys used to stabilize them.

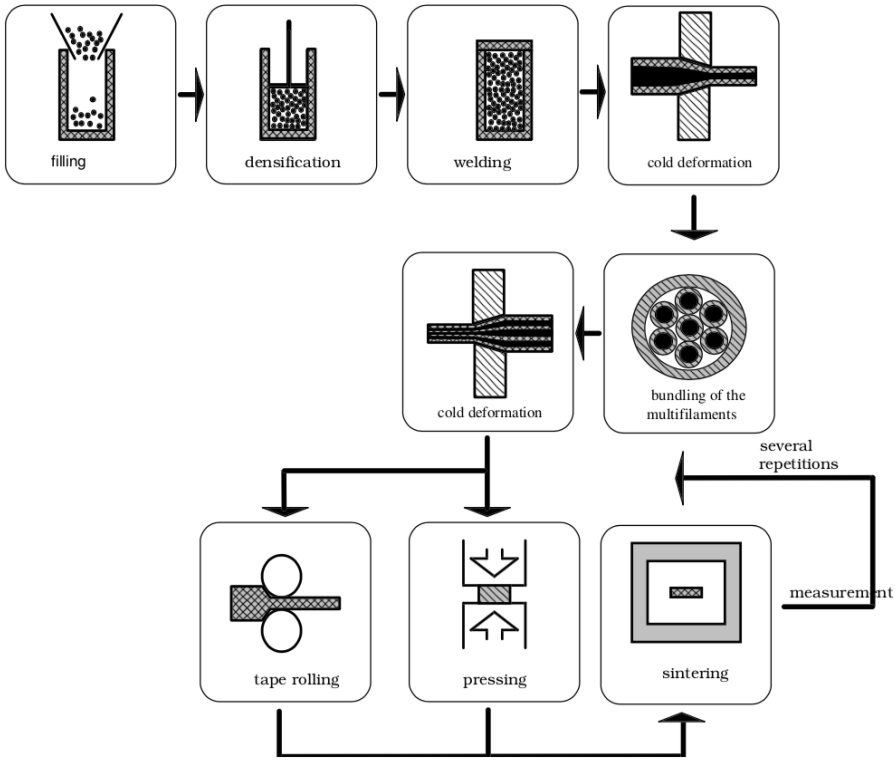

Figure 2.4: A schematic outline of the PIT process used to manufacture LTS wires and cables, as well for HTS multifilamentary wires, strands and tapes. Taken from Lehndorff (2001).

This fabrication process uses also sufficient cold work and multifilamentary extrusion as seen in Figure 2.4, and a cross-section of Bi-2212 multifilamentary round wire manufactured by Oxford Superconducting Technologies (OST) company is shown in Figure 2.5 where superconducting filaments and silver sheath are observed.

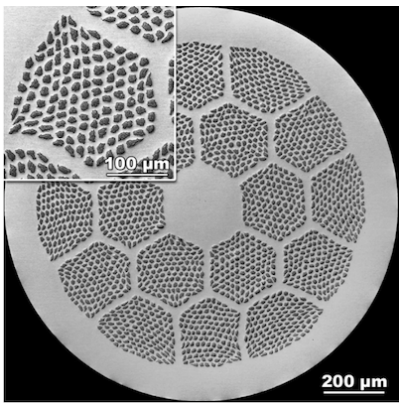

Figure 2.5: Cross-section of a Bi-2212 multifilamentary round wire manufactured by OST company. Taken from De Marzi et al. (2016).

- ***Tapes***

Two kinds of tapes are currently available in the market and are differentiated by HTS used and the fabrication process involved (De Marzi et al., 2016; MA, 2004; Senatore et al., 2014):

i. The first kind is known as the first generation (1G) HTS tapes and uses BSCCO materials, the Bismuth-Strontium-Calcium-Copper-Oxide, (Bi, Pb)$_2$Sr$_2$Ca$_2$Cu$_3$O$_{10-x}$ (Bi-2223) variant, essentially.

   Bi-2223 tapes use pure powders of Bi-2212 phase and other precursor oxides, packed using PIT techniques combined with overpressure methods and silver alloys sheaths as a stabilizer. This allows better flexibility and mechanical robustness characteristics, e.g., more feasible for coils and power transport cables. However, this kind of tapes tends to be more sensitive to magnetic fields, especially the perpendicular components which leads to great current density degradation (Pina, 2010). Figure 2.6 shows the cross-section of a 1G tape obtained by this methodology;

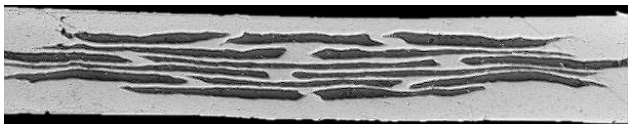

Figure 2.6: An optical micrograph with the cross-section of a 1G tape using Bi-2212 materials manufactured by Beate Lehndorff at CryoElectra GmbH, showing a matrix of 15 superconducting filaments inside a silver sheath. Taken from Lehndorff (2001).

ii. The second kind is known as the 2G HTS tapes, or simply Coated Conductors (CC), and uses YBCO materials. In this kind of conductors, PIT techniques cannot be used[11] due to a more pronounced crystal grain misalignment in YBCO materials,

[11] According to De Marzi et al. (2016) and Lehndorff (2001), one of the reasons that PIT technique cannot be used to manufacture CC, is due to platelet structure of micro crystals inside the microstructure during its deformation because they do not glide over each others so easily, thus not favouring the texture formation.

nor is e.g., possible to obtain round cables from it. Instead, techniques as thin epitaxial films deposited onto flat and flexible metallic tapes coated with buffering metal oxides and stabilizing layers are used to prepare high-performance superconducting conductors. An illustration of a layered architecture CC commercialized by SuperPower company is shown in Figure 2.7, aims to demonstrate this methodology.

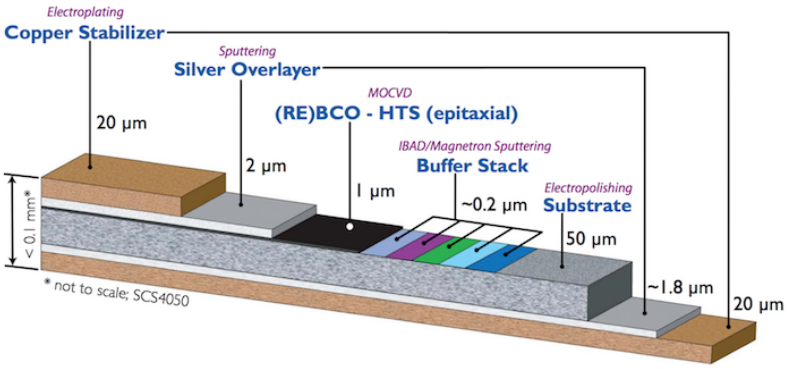

Figure 2.7: Generic schematic of a layered architecture for a Coated Conductor manufactured by SuperPower Inc. company. Taken from SuperPower-Inc. (2014).

CC due to its improved properties, such as the mechanical robustness, operation at a higher magnetic field and critical current is considered more relevant for the planned work of present thesis.

2.2.2 Applications of HTS Materials

Superconducting materials, in general, can be used in many practical applications and its use has been growing over the years.

LTS materials have been dominant in the market with steady growth, mostly in health applications using high field magnets for Magnetic Resonance Imaging (MRI) and Nuclear Medical Resonance (NMR). Research in high energy physics for complex systems like the Large Hadron Collider (LHC) at CERN or the Facility for Antiproton and Ion Research (FAIR) in Darmstadt, Germany, are other areas of strong applicability, as are the nuclear fusion in projects like the International Thermonuclear Experimental Reactor (ITER), Wendelstein 7-x and others.

HTS materials due to their advantages have a growing share in the market. Applications like passive high-frequency and microwave devices constituted by YBCO thin films in the electronics field, or the materials characterization, scientific instrumentation and geophysical exploration using Superconducting Quantum Interference Devices (SQUIDs) magnetometers due to its ultra-high magnetic field sensitivity, are just a glimpse of the broader spectrum of possible applications (Luiz et al., 2011; Pina, 2010; Seidel, 2015).

Processing machines and the transportation area where Magnetic Levitation (MagLev) projects are taking major advances are other applications in the industrial field, in addition to, new medical applications or the main purpose here, in the power energy field. Table 2.2 aims to give an overview of some applications where HTS materials are currently emerging.

Table 2.2: Emerging Industrial and Energy applications for HTS materials, according to CONsortium of European Companies determined To Use Superconductivity. Adapted from Conectus.org (2018).

Application	Major Technical Features	Additional Benefits
Power Cables	Higher current densities Lower conductor diameters Smaller transmission losses	Lower voltage level No heat emission No external **E** or **H** fields (design dependent) Eco-friendliness due to Oil free
Fault Current Limiters	Highly non-linearity (due to super-normal-conductor transition) Self-controlled current limitation	Fail-safe (no external trigger necessary) Automatic self-recovery Ultrafast (react in 1-2 milliseconds)
Motors and Generators	Higher power densities Higher magnetic fields Smaller size Lower weight Lower losses	Higher efficiency under partial load operation
Transformers	Higher current densities Smaller size Lower weight Lower losses	Eco-friendliness due to Oil free
Magnetic Bearings (based on HTS bulk materials)	Self-centering bearing Frictionless Free gap	Passive devices Soft bearing characteristics No additional active monitoring and control system
Flywheel Storage Systems	Energy storage with high power density Energy storage with high cycle efficiency	Vacuum compatible Losseless Passive frictionless bearing

2.3 Coated Conductors

Superconductivity effect is strongly anisotropic owing to grain boundary orientation of polycrystalline material. Thus, for an increasing misorientation of angles between adjacent crystallites, the superconducting currents are easily interrupted at interfaces between the crystals of superconductor, which leads the critical current density falling off exponentially. However, in tape form, these materials still present high-performance superconducting properties (De Marzi et al., 2016; Lehndorff, 2001; Saxena, 2010).

2.3.1 Manufacturing Process

CC manufacturing is accomplished by a thin film technology, which is justified by the fact that film texture can be reliably controlled through an epitaxial process, achieving the best J_c for this type of tapes. In a brief, the manufacturing process consists mainly of two stages according to De Marzi et al. (2016) and Senatore et al. (2014, 2016):

i. Preparation of textured template, which includes buffer layers to prevent metal elements diffusion into the superconductor during high-temperature processing (MA, 2004). This is achieved by two approaches, through Rolled Assisted Bi-Axially Textured Substrates (RABiTS) or Ion Beam Assisted Deposition (IBAD);

ii. Deposition of a superconducting active REBCO layer on the template. This process can be achieved by several techniques, and the most used in the manufacturing industry are either by chemical processes as Metal-Organic Deposition (MOD) and Metal-Organic Chemical Vapour Deposition (MOCVD) or by physical techniques as Reactive Co-Evaporation (RCE) and Pulsed Laser Deposition (PLD).

These two stages are completed with the addition of silver and copper thick layers, which completes the conductor providing environmental protection and thermal stabilization, respectively. Figure 2.8 illustrates briefly these two main approaches used by the superconductors manufacturing industry.

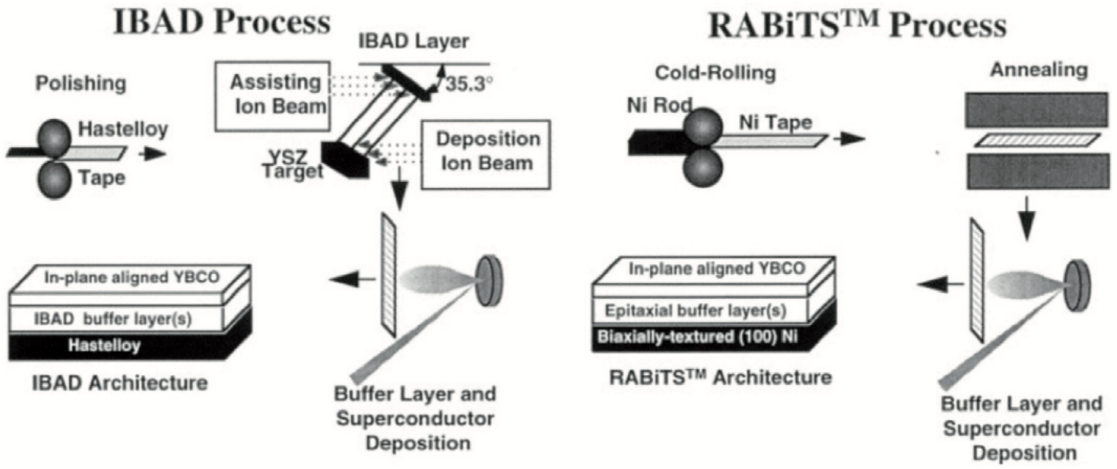

Figure 2.8: A summarizing schematic of manufacturing methods for 2G CC, IBAD (left) and RABiTS (right), respectively. Taken from Celentano and Augieri (2012)

- ***RABiTS process***

Rolled Assisted Bi-Axially Textured Substrates approach consists of the deformation of a NiW metal alloy substrate (with reduced magnetization and higher mechanical strength) through processes of rolling and recrystallization annealing. Followed by deposition of epitaxial buffer layers of Y_2O_3, CeO_2 and Yttrium-Stabilized Zirconia (YSZ) onto the textured NiW substrate, serving to block the inter-diffusion of substrate atoms and to provide lattice match for the growth of superconducting layer.

Currently, instead of NiW metal alloys, developments are being oriented towards substrates characterized by reduced ferromagnetic behaviour to minimize losses by hysteresis especially for power applications (Senatore et al., 2014).

- ***IBAD process***

Ion Beam Assisted Deposition use stainless steel or polycrystalline Hastelloy tapes submitted to an electropolishing process. A diffusion-barrier layer of Al_2O_3 and a seed layer of Y_2O_3 are deposited onto the surface of the metallic substrate by a sputtering technique, followed by the deposition of a biaxially textured layer of MgO with an assisting 1 keV Ar^+ ion beam in a standard PLD geometry.

IBAD process reduces the surface roughness from ~50 nm to less than 2 nm, generating a preferred texture in the buffer layers. Is the most used by current manufacturers. Table 2.3 gives an overview of these superconductors manufacturers and the main processes applied.

Table 2.3: Fabrication key parameters for CC among the industrial superconductors manufacturers. Adapted from Senatore et al. (2014, 2016)

Manufacturer	Technique	Substrate	Buffer layers	HTS active layer	Cu stabilizer
AMSC	RABiTS/MOD	NiW	$Y_2O_3/YSZ/CeO_2$	Y123	laminated
SuperPower	IBAD/MOCVD	Hastelloy	$Al_2O_3/Y_2O_3/MgO/LaMnO_3$	Gd123	electroplated
Bruker	ABAD/PLD	Stainless steel	YSZ/CeO_2	Y123	electroplated
Fujikura	IBAD/PLD	Hastelloy	$Al_2O_3/Y_2O_3/MgO/CeO_2$	Gd123	laminated
SuperOx	IBAD/PLD	Hastelloy	$Al_2O_3/Y_2O_3/MgO/LaMnO_3/CeO_2$	Gd123	electroplated
SuNAM	IBAD/RCE	Hastelloy	$Al_2O_3/Y_2O_3/MgO/LaMnO_3$	Gd123	electroplated

For a larger commercial diffusion of CC, manufacturers are focusing on some important aspects which can not be dissociated, namely:

i. Performance of produced tapes, which shows large variability when comparing from different manufacturers at temperatures of 77 K in self-field and at 4.2 K in high-field (i.e., 19 T), without univocal correlation between critical current values (Senatore et al., 2016);

ii. Length of manufactured tapes, owing to the demand of different sectors. At the electric utility sector there are no rigorous requirements concerning a single-piece length, the coil manufacturers, on the contrary, demands longer pieces of tapes with enhanced mechanical properties.

   Bruker company, e.g., produces 12 mm wide tapes up to 300 m length with I_c of 420 A (at 77 K, self-field). However, there is a consensus for the energy sector that more than 1000 m are necessary for applications like SFCL, transformers, industrial motors or generators according to Celentano and Augieri (2012) and MA (2004). Besides, hundreds of kilometres of tape are necessary to build a 1 km long power cable according to Senatore et al. (2014);

iii. Tape's price is another key factor considering that CC costs are essentially due to large investments in research and production infrastructures. In addition, power

devices manufacturers demand prices four times less than practised. Thus, there is a clear conviction that an improvement on current methods and a more efficient production will result in a reduction of tape's final price.

2.3.2 Coated Conductors Constraints

CC in the market are characterized by a diverse constitution and obtained with different combined techniques as seen in Table 2.3. In particular, an interior REBCO layer of intrinsic brittleness is used, presenting different mechanical and electromechanical properties. Therefore, it is important to address some situations which can lead to partial or complete damage considering the involved strain when in operation. Figure 2.9 illustrates different types of strain which a CC tape can be subjected.

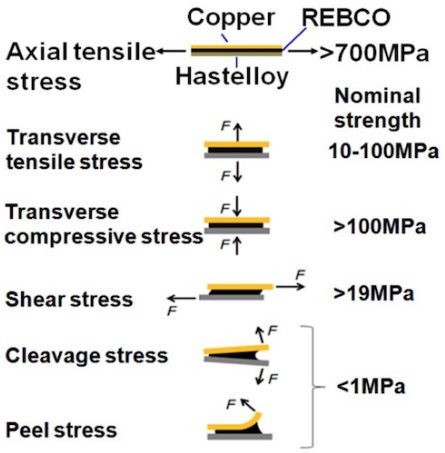

Figure 2.9: Illustration of different strain types and mechanical strength on a Coated Conductor. The stress values correspond to a tape with electroplated copper stabilizer. Taken from Maeda and Yanagisawa (2014).

Manufacturers already offer tapes with good mechanical strength, but as illustrated in Figure 2.9, CC present an anisotropic mechanical strength. As a result, important care must be taken in order to avoid damages at the superconducting layer when handling the tapes.

Supported on what is summarized in Figure 2.9 and according to Barth (2013), Maeda and Yanagisawa (2014), and Senatore et al. (2014), the following aspects should be considered when using CC:

i. In the transverse direction, tensile strength assume low values between 10-100 MPa, and it can introduce a problem owing to the forces acting to the normal direction of the tape surface;

ii. Cleavage strength (due to external forces acting to open one edge of the adhesive assembly) and peel strength (similar to cleavage with the exception that only one part of the adhered tends to be flexible) are extremely weak;

iii. Critical axial tensile stress, depending on the copper fractional area in commercial available electroplated CC can be higher up to 700 MPa, superior to 430 MPa presently supported in BSCCO tapes with new lamination techniques;

iv. Tapes laminated with materials of large thermal contraction allows the highest strain limits (Senatore et al., 2014);

v. Delamination[12] at the interface between layers of CC can occur when applied a sufficient strain, and these consequences are mentioned in literature by several authors, e.g., in Barth (2013) and Senatore et al. (2014).

Devices like Walters Spring (WASP) are used to measure the strain dependence of critical current of superconductors with relatively long length. For this purpose, the superconductor is wound along the outer surface of a spring in which a torque is applied, resulting in an axial strain over the superconductor (Barth et al., 2015; Sugano et al., 2008);

vi. The electromagnetic strain[13] may degrade irreversibly the critical current of CC during operation. Observe that, conductors hoop stress[14] can limit the overall current density on HTS applications, if not limited in 500-700 MPa range, e.g., a REBCO NMR coil is subjected to enormous longitudinal stresses, $\approx$ 500 MPa (Barth et al., 2015; Barth, 2013; Maeda and Yanagisawa, 2014);

Summarizing, along with the magnetic field and the operating temperature, the mechanical strain also influences the superconductor's current carrying capabilities.

2.4 Coils from Coated Conductors

Coils represent an important part for the construction of different HTS devices, and several topologies have been advanced. This section describes the necessary steps found in the literature to build coils, including the cut of tapes and the necessary joints to splice and finish.

Magnets have been along the years a great booster in the development of coils using HTS materials, where aspects like the winding process, coil impregnation and insulation, pose great challenges, as do the cut and joint process.

[12] Delamination has not been reported as a problem for Bi-2223 tapes, despite the lower strength values showed in tests when comparing against CC, according to Senatore et al. (2014).

[13] Note that, Lorentz forces affect the conductor longitudinally in tension.

[14] Hoop stress is the axial tensile along the longitudinal direction of the conductor in solenoidal magnets. Therefore, the conductor substrate metal should be strong enough to bear most of this stress in order to limit the strain on the superconducting layer.

2.4.1 Winding Processes

Two main techniques have been used to wind HTS high-field magnets along the years, namely, Layer-Wound (LW) and Pancake or Double-Pancake (DP):

i. LW technique, use a single conductor piece which is wound from the innermost to outermost layers, turn by turn one layer at a time;

ii. DP with the height of twice the tape width, two pancakes are wound sequentially from a midpoint of the conductor, spiralling radially outward from the innermost to outermost turns, and the *cross-over* from one pancake to other occurring at the innermost turns without interruption (Senatore et al., 2014).

Certain constraints must be taken into account as seen in section 2.3.2 when using CC. The winding process can introduce bending strains which can occur along the conductor axis and known as *easy bending* or normal to the conductor axis known as *difficult bending*, e.g., at the inner transition region in a DP coil or each end of an LW coil. Therefore, for large winding diameters there is no big issue, on the contrary, for diameters less than 50 mm, some design constraints are imposed.

In addition to usual winding techniques, new configurations have been studied and tested. Figure 2.10 shows in (a) a short-circuited DP coil made with CC by a No-Insulation (NI) winding technique. It was developed by Qu et al. (2016) to test a Persistent Current Mode (PCM) switch to be used in high-field HTS magnets, e.g., NMR and MRI, instead of driven mode operation in which these applications operate when using REBCO magnets. In (b) a schematic panoramic view illustrates the resistive pancake-pancake (P-P) joint between top and bottom pancakes terminals.

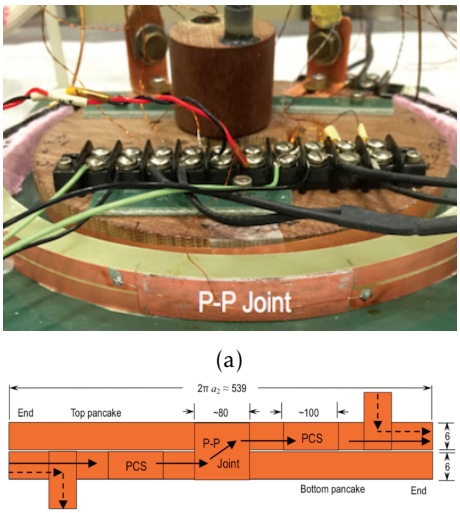

(a)

(b)

Figure 2.10: (a) short-circuited DP coil wound by NI winding technique mounted to test the (P-P) resistive joint; (b) schematic panoramic view illustration of the coil. Taken from Qu et al. (2016).

A low-resistance HTS short-circuited coil using the LW technique is shown in Figure 2.11. It was developed by Murta-Pina et al. (2018) using a new engineering design that allows a single joint independent from the number of turns and is intended for medium voltage applications such as SFCL where a short-circuited HTS secondary is used.

Figure 2.11: A low-resistance HTS short-circuited coil using the LW technique and made with CC. Taken from Murta-Pina et al. (2018).

Figure 2.12 shows in (a) a ring-shape 2G HTS magnet inspired in the *wind-and-flip*[15] method proposed by Sheng et al. (2017). This approach uses a stack of ring-shaped CC to build trapped-field magnets and is intended to provide feasible sizes according to the pieces of tape used and the slits made on it to achieve the desired diameter.

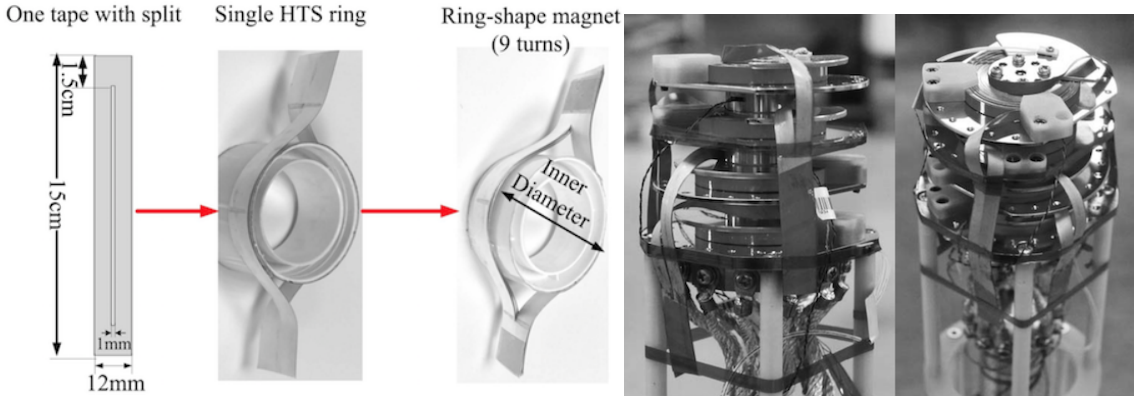

Figure 2.12: Jointless continuous HTS coils: (a) a ring-shape 2G HTS magnet, adapted from Sheng et al. (2017); (b) a DP coil using a single CC split into two tapes and wound by the *wind-and-flip* method, adapted from Kim et al. (2015).

In (b) a DP coil without any electric joints proposed by Kim et al. (2015) is shown. It uses a single wide CC split longitudinally in the middle as shown by the schematics illustrated in (a). This coil is wound by the *wind-and-flip* method and was proposed to be used in PCM operation on magnets, i.e., NMR and MRI applications, as in SFCL, nevertheless, are not scalable for medium voltage devices (Murta-Pina et al., 2018).

[15] Wind-and-flip is a method intended to avoid non-superconducting joints and consists of a closed loop for the current created by longitudinal partial slices in CC. For this purpose, each slice is wound in a coil shape and one of the coils is flipped to avoid field cancelling. Detailed information on this method can be found in Seyeon Lee et al. (2013) and Woo-Seok Kim et al. (2009).

- ***Coil Impregnation and Insulation***

Coils can be constructed with or without impregnation. Impregnation permits to fill a void-filled winding into a solid monolithic structure, with the advantage of mechanically stabilize the conductors distributing equally the loads along the axial direction. Therefore, helping to immobilize against electromagnetic forces.

Impregnation is done by using glues, epoxy resins, waxes, paraffin and solders. In brief, materials[16] with extremely low thermal contraction, allowing the reduction of thermal stress on the edge of superconductors due to the mismatch of the thermal contraction coefficients among the impregnation materials and CC (Barth, 2013; Goldacker et al., 2014; Senatore et al., 2014).

For the insulation, which prevents the current from passing between the conductor's turns, CC manufacturers suggest *Kapton* tape, but the use of enamel (used for insulation of NbTi wires) is also recommended on the literature. According to Badcock et al. (2009) and Senatore et al. (2014), the UV curable varnish is also used to insulate slitted strands of Roeble cables, and also thermally-cured and UV-cured polymer coatings, oxide physical vapour deposition, oxide sol-gel coating, polyester heat-shrink tubing and the electrodeposited polyamide insulation are some of the other insulation techniques tested.

2.4.2 Cutting Methods

In order to avoid some of the issues described in section 2.3.2, the most indicated methods must be considered to cut the CC, since the layers of superconducting material (ceramic and brittle) under the protection of substrate and stabilizer layers can be damaged. For this purpose, some of the methods found in the literature are described in this section as follow:

i. Laser cut with conventional machines uses heat to melt the material and has been used for many years to cut several types of materials with good flexibility, results and cutting rates, including ceramic, composites and laminated materials. However, owing to heating and melting defects imposed by the laser it does not show good results when used to cut coated conductors.

   Another laser variant tested is the picoseconds-infrared laser technology, which permits to avoid defects on the tape, but it is not appointed as economically viable in terms of production speed (Goldacker et al., 2014);

[16] Observe that, materials used for impregnation and into coated conductors can expand if heated or contract if cooled, causing a certain deformation of its lattice and resulting in thermal stresses. Additionally, a mismatch of the thermal expansions of the materials during the cool down process can result in damages on REBCO tapes, which may lead also to the degradation of current carrying capability.

ii. Electrical Discharge Machining (EDM) tested and reported by Senatore et al. (2016) to cut tapes with laminated stabilizers, reducing till 2 mm width of tape with a single cut from one side, can also be considered depending on the tapes' structure. This technique creates sparks that melt tiny portions of the material without generating cutting forces. It is a useful approach but requires electrically conductive materials;

iii. Water jet cut uses supersonic erosion to remove the material, using or not an abrasive (usually for tougher materials) and is one of the most versatile and fastest cutting processes in use at Industry. This process presents as advantages, the cold cutting, i.e., no heat affected zone, low stress, no warp on the material and is considered environmentally friendly. At present, there are no records on literature referring strictly the use of this cut method for CC without the addition of any other technique;

iv. A technique tested by Heilmann (2013) combines both water jet and laser cut. A fibre-coupled pulsed diode pumped solid state laser is combined with a water jet guided system, in order to minimize the burr height and the heat caused by the laser during the cut. This is an elaborated process where parameters as the laser power and repetition rate, the tape velocity through the machine and the water pressure need to be carefully chosen and optimized in order to obtain good cut results. Nonetheless, the authors report critical current losses of 16% in tapes cut by this method when compared with untreated tapes.

v. Mechanical punching technique is identified by the Karlsruhe Institute of Technology (KIT) and the Industrial Research Limited (IRL) as the more suitable method to cut CC according to Badcock et al. (2009) and Goldacker et al. (2014).

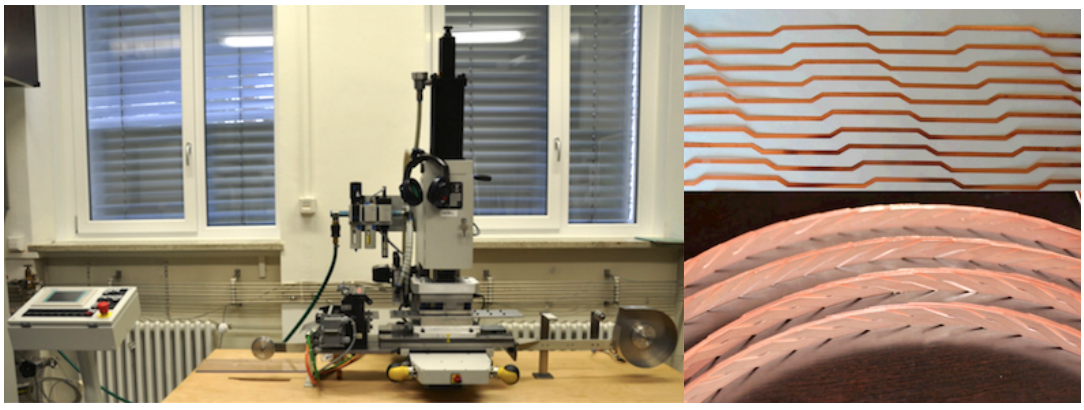

(a) (b)

Figure 2.13: Fabrication of Roeble cables by the mechanical punching technique. Adapted from Goldacker et al. (2014): (a) A reel-to-reel computer-controlled pneumatic punching machine at KIT to produce Roebel strands; (b) Ten strands punched from a 12 mm wide CC (top), Assembled Roeble cables from the strands (bottom).

This technique uses a reel-to-reel computer-controlled pneumatic punching tool, shown in Figure 2.13. As advantages, allows high-speed production of strands with good precision, i.e., typically 50 m of tape per hour with less than 50 μm of loss at each slit, flexibility and the possibility to adjust the tool for different cut geometries, producing strands with current carrying capability losses less than 2-3% for homogeneous CC (Goldacker et al., 2014).

Several Roeble cables which are made by meander-shaped CC strands and assembled as shown in Figure 2.13 to reduce induced eddy currents, current loops and consequently the ac losses on power cables, use this punching technique to obtain the desired strands.

vi. A less elaborated method, such as a regular stainless-steel electrician scissor was also tested by Murta-Pina et al. (2018) with good results for the final critical current measured on tapes cut by this method, showing no visible delamination. Nevertheless, for large-scale cutting processes, it is not feasible.

2.4.3 Junction Methods

Joints pay a key role to obtain good superconducting devices, which require electrical connections between superconductors and other parts that constitute them. Several studies found in the literature focus on the development of good techniques to bond the CC in order to achieve excellent joints.

- ***Types of joints***

According to Brittles et al. (2015) and Kato-Yoshioka et al. (2006), these techniques can be classified as superconducting or non-superconducting joints:

i. Superconducting joints use direct bonding approaches such as the solid state diffusion under uniaxial pressure, melting and melting-diffusion. These techniques involve high temperatures, followed by a prolonged oxygenation-annealing process to recover the degraded superconducting properties of HTS layers, which lose oxygen at high temperatures due to its crystalline nature (Barth, 2013; Brittles et al., 2015; Senatore et al., 2014).

An excellent result for a superconducting joint was reported by Park et al. (2014), it is based on atomic diffusion with partial melting of internal REBCO layers in the CC and was accomplished by a series of processes, namely:

a) Removal of stabilizer layers by a chemical etching to access the REBCO layer;

b) Micro-holes by laser on tape to facilitate oxygen diffusion;

c) Heat treatment for joining in vacuum at a peak temperature of 850°C;

d) Oxygenation annealing under high-pressure oxygen at 500°C to increase the oxygen content of the REBCO layer and restore its superconducting properties.

As a result, it allowed the establishment of a resistance-free closed loop for PCM operation, steady for 240 days with total circuit resistance of $<10^{-17}\Omega$ (i.e. perfect electrical connection).

ii. Non-superconducting joints (also known as resistive joints), on the contrary, allow more flexible geometries and use a low melting point metal as a soldering material, filled between the contact area of the tapes.

This approach is expected to result in a higher joint resistance value, owing to the sum of resistances of soldering material and tape stabilizing layers. Thus, the joint resistance using this technique varies over orders of magnitude, depending on tape and solder types used in the joining process. According to Senatore et al. (2014) values of specific resistivity, i.e., resistance times joint area, between 30-500 $n\Omega cm^2$ and measured at 77 K, are reported as good ones.

The main types of configurations used to build joints using the techniques presented above are illustrated in Figure 2.14, where a schematic of a non-superconducting joint is indicated for both lap and bridge configurations.

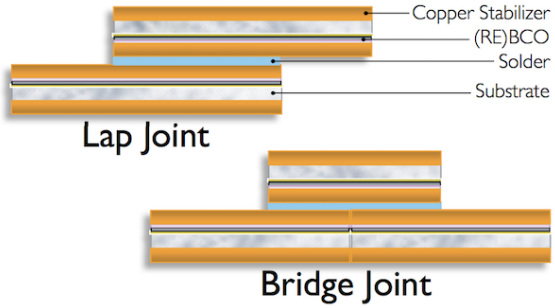

Figure 2.14: Original schematic of the main types of joint configurations in use (lateral view): (top) lap joint and (bottom) bridge joint. Taken from SuperPower-Inc. (2014).

A study developed by Duckworth et al. (2010) with the objective to verify a reproducible method to obtain low-resistance and high-mechanical-strength joints, appoints that joints of lowest resistance (e.g., between 20-100 nΩ in 4 mm width tapes) are influenced by the tapes' orientation in the joint and its stabilizers material, i.e., best results with electroplated copper stabilizer, see Table 2.3 for reference.

Another factor usually considered, is the solder applied on tapes through the superconductor side, rather than the substrate side, i.e., in a face-to-face configuration. With the lap configuration producing the best results according to AMSC (2012).

Optimization of CC is a constant goal for manufacturers, who align the superconductor layer in a longitudinal way on tapes in order to make the current flow easily. Considering this factor, a conceptual sketch of bridge joint variants is illustrated in Figure 2.15 from a study developed by Chang et al. (2011) on the effect of the direction of the joints in HTS applications such as NMR, where it is important to ensure the homogeneity of the magnetic field.

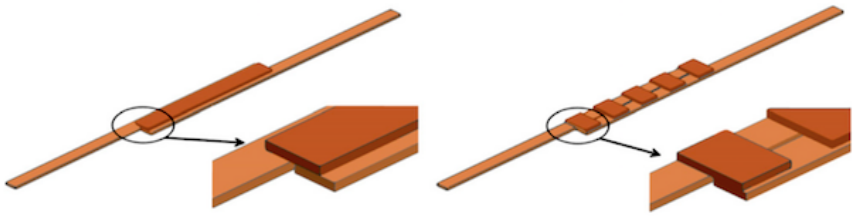

Figure 2.15: Sketch of bridge joint variants: (left) parallel direction (PD joint) with the CC and (right) orthogonal direction (OD joint) relative to the CC. Adapted from Chang et al. (2011).

In this study, the auxiliary pieces of the tape were overlapped in a parallel or orthogonal direction to CC, achieving joint resistances between 40-140 nΩ. Therefore, three important remarks from this study:

a) Considering the same overlap tape width, bridge joints in parallel direction offer better results rather than in orthogonal;

b) The narrower the overlapping tape, the lower the joint resistance;

c) Lap joints produce better results than bridge joints, in terms of joint resistance and critical current.

- ***Temperature and applied Pressure***

During the joining process, temperature and the applied pressure on the contact area are important aspects to consider also, in order to obtain a low joint resistance preserving the superconducting properties of the tapes in contact.

As exposed in section 2.3.2, it is important not to exceed the transverse stress limits of the CC, and there are guidelines from AMSC (2012) and SuperPower-Inc. (2013) on how to perform low-resistance splice joints with recommendations for temperature thresholds on these procedures.

A study developed by Bagrets et al. (2015) on the dependence of joint resistance with the applied pressure for non-superconducting joints, appointing two types of contacts:

a) Soldered joints, between tapes (with applied pressures till 10 MPa);

b) Mechanical pressed (also mechanical joints), with applied pressure till 25 MPa. Useful for stacked tapes inside HTS cables.

Some examples of devices found in the literature and used to make joints between tapes are shown in Figure 2.16.

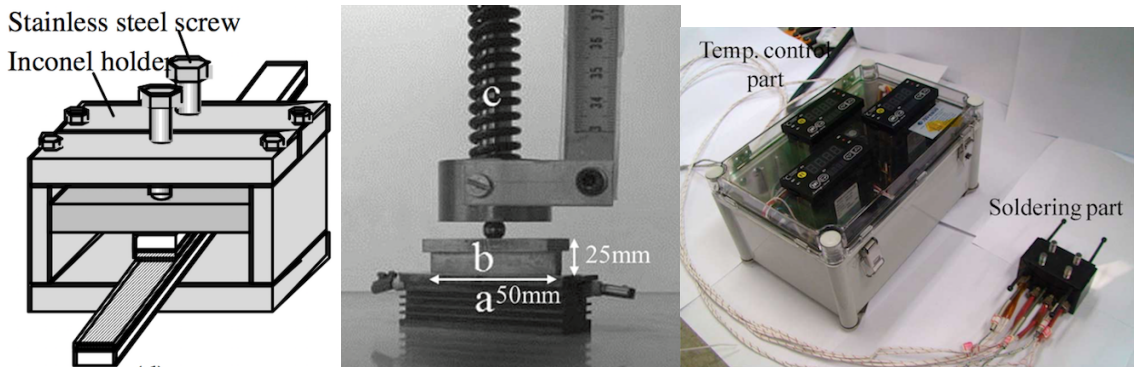

(a) (b) (c)

Figure 2.16: Different kinds of soldering devices used to make joints: (a) Schematic of a holder device, adapted from Kato-Yoshioka et al. (2006); (b) A soldering device, adapted from Bagrets et al. (2015); (c) A soldering machine with real-time temperature control, adapted from Ki Sung Chang et al. (2010).

In (a) a holder device made of Inconel used by Kato-Yoshioka et al. (2006) for joining by diffusion. Joint resistances between 0.02-0.03 $\mu\Omega$ for a joint area of 40 mm^2 were achieved with an applied pressure (controlled by torque on the screws) between 10-60 MPa at room temperature. They also registered a decrease of the critical current for an applied pressure above 30 MPa.

In (b) a soldering device with resistive heating on base, pressuring punch and spring to control the applied pressure used by Bagrets et al. (2015), which appoint the range 5-10 MPa as reasonable values to achieve a low-resistance contact.

In (c) a soldering machine developed by Ki Sung Chang et al. (2010), to make joints on various bending diameters (100-150 mm), is comprised of a temperature control part with thermal sensors and cartridge heaters which control, monitor and adjust the temperature in real-time, and a soldering part where the heat and pressure are applied.

- ***Soldering Materials***

For the realization of non-superconducting joints, the soldering materials can be acquired in different forms, e.g., powders in-tube, ribbon solder or premixed. The choice of which one to use is according to practical application, and the preference should take into consideration the following aspects:

a) A low melting point, in order to bond the tapes with a lower possible temperature;

b) Lower electrical resistivity, to get the best electrical connection between the superconductors;

c) Higher thermal conductivity, to ease the heat transfer between the CC and rest of the components in the systems where it is inserted;

d) Similar thermal expansion coefficients, since a large mismatch of the coefficients between the CC and soldering materials, can cause stresses, thus damage the CC.

The use of premixed solder pastes or ribbon solders helps to accomplish more homogeneous resistive joints. According to Senatore et al. (2014), the best results are achieved with two-component alloys (e.g., SnAg, InSn, SnPb), with tin and lead prices per gram as the cheapest in the market (Tsui et al., 2016). Table 2.4 lists some lead-free solders compositions usually recommended by manufacturers for low-resistance joints.

Table 2.4: Recommended solders compositions by manufacturers, Pb-free.
Information adapted from (Indium-Corporation, 2016).

Composition (%)	Melting Temperature (°C)	Electrical Conductivity (% of IACS)	Thermal Conductivity (W/cm°C @ 85 °C)	Thermal Coefficient of Expansion (PPM/°C @ 20 °C)	Tensile Strength (MPa)
100In	157	24.00	0.86	29	1.88
52In 48Sn	118	11.70	0.34	20	11.86
96.5Sn 3.5Ag	221	16.00	0.33	30	39.99
96.5Sn 3.0Ag 0.5Cu	220-217	-	-	-	49.64

2.4.4 Applications of HTS Coils

The HTS materials as exposed in Table 2.2 have many applications in the industrial and energy sector, and HTS coils, in particular, can be used in power applications such as the SFCL, detailed as follows due to its specific interest for the present thesis.

SFCL are devices with intrinsic non-linear resistivity owing to the HTS materials which constitute it, acting as a natural fault current limiters. Such devices present a negligible impedance in normal conditions where it can carry high current densities (i.e., in superconducting state), whereas in cases of currents above a certain threshold (e.g., under a fault) its state switch to a higher impedance due to the loss of superconducting properties (i.e., normal state). Nevertheless, It returns to normal conditions once the fault is suppressed (Pina et al., 2010).

These devices in nominal conditions, when included in an Electric Power Grids (EPG) contribute to transient stability of the generators, thus for global stability of the grid owing to the good transition from the superconducting to resistive or inductive states in fault situations. This behaviour allows a reduction of short-circuit currents in the order of 20-50% within milliseconds, whereas 30% is already considered an adequate safety margin for the network types of equipment (Didier and Lévêque, 2014; Didier et al., 2015).

Amongst the different SFCL, the emphasis goes to resistive and inductive topologies, mature technologies with several practical applications mentioned in the literature.

Resistive Superconducting Fault Current Limiters (rSFCL) present their compactness as an advantage because HTS elements are in series with the grid, allowing fast limiting action and recovery in order of a few seconds. However, several HTS elements must be connected in series to reach the desired resistivity specifications, and connections from normal conductors to superconductors materials are necessary, leading to ohmic losses and the necessity of current leads.

Inductive Superconducting Fault Current Limiters (iSFCL) on the other hand, are magnetically linked with the grid operating as a current transformer with short-circuited secondary built form HTS elements. In this topology, the primary and secondary embrace an iron core concentrically, forming a closed or open path for the magnetic flux. An illustration of the electrical diagram of an iSFCL is shown in Figure 2.17.

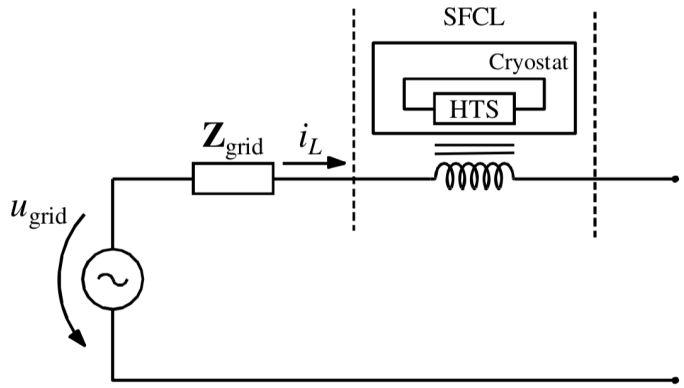

Figure 2.17: Electrical diagram of an Inductive Superconducting Fault Current Limiter iSFCL. Taken from Pina et al. (2010).

In normal operation conditions, the iron core is magnetically shielded by the induced currents in the superconductor as a result of the primary's magnetic flux induction. Whereas, under fault conditions an abrupt increment in the line current occurs, leading the HTS coils to lose its superconducting state, ceasing the shield of the flux, which follows then to a preferential path through the iron core being amplified, increasing consequently the inductance and limiting the current (Pina et al., 2010).

Some main advantages of iSFCL over the rSFCL are its impedance that can be adjusted through the primary turns, no need for current leads, thus, no ohmic losses and hot spots easily suppressed by cryogenics. Nevertheless, it is much heavier and bulky because of the iron core, since for an air core option creates a weaker inductance in the line under fault situations, resulting in an inefficient limitation of the current.

Researches with the objective to reduce the need for an iron core have been developed, and Qiu et al. (2018) fabricated a two-winding structure air-core iSFCL prototype, shown in Figure 2.18, with a primary copper winding and a secondary with four independent

NI winding using CC. Results show a good prospect to use such architecture since it was able to limit the fault current from 3.3 kA peak to 478 A.

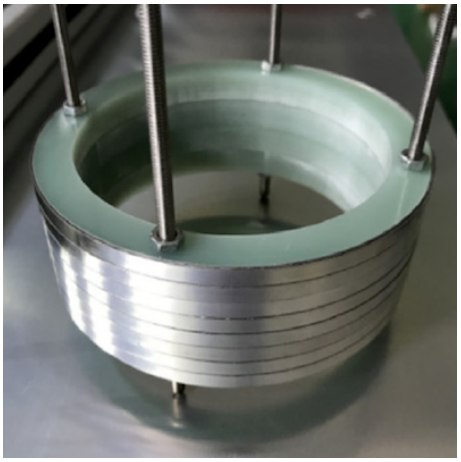

Figure 2.18: No-Insulated coil made of CC for the secondary of an air core iSFCL. Taken from Qiu et al. (2018).

2.5 Synopsis

In this chapter, a literature review was addressed on some of the most relevant introductory topics for a theoretical understanding of the thesis subject, namely, a brief history of superconductivity followed by the most important properties of superconductors and their characterization.

The most relevant HTS materials commercially available, and the various applications, were discussed.

Next, the CC were addressed in more detail, describing the fabrication processes and the constraints they present for practical applications.

Finally, the use of CC to build HTS coils was discussed, followed by the winding processes, the tested cutting methods, the essential joints types and processes, and the practical applications for these coils.

3 Analysis of the Tapes Cutting Process

This chapter will present the required steps for prototype development. For this purpose, experimental procedures concerning the cut of tapes will be exposed in detail, the critical current of tapes after the cut will also be measured and the results are presented and discussed.

3.1 Design of the HTS Coils

Several applications which make use of coils from HTS materials usually requires non-superconducting joints, hence additional points of ohmic losses are inevitably inserted for each joint. Therefore, it is important to find ways to reduce these losses, especially for real scale power applications where devices efficiency must be a constant concern.

Along the literature, there are some examples of these efforts as exposed in section 2.4.1 where a new engineering design of a low-resistance short-circuited HTS coils was proposed and validated experimentally by Murta-Pina et al. (2018). Therefore, the aim of the present thesis is to contribute to the optimization of this design and find feasible solutions to manufacture these low-resistance short-circuited coils.

The required parameters to be considered for this design from a single tape are detailed in Table 3.1 and the necessary steps to build the coils are described as follows:

i. The process starts by defining the required number of turns N to be obtained from a tape with given length L and width W;

ii. The tape is cut through its middle axis removing slices of lengths d and d_3 with W_1 width, as shown in Figure 3.1 b) where a meander cut angle θ of 90° is considered hence d_3 turns out null and Figure 3.2 (a) where for $\theta < 90°$ the distance d_3 takes a considerable value during the cut process of the tapes.

   Since the length d of slices to be removed and total length L of the tape that builds the coil are dependent on the required number of turns N. Consequently, these

distances are governed by the following equations, considering the thickness δ (i.e., the tape plus applied insulation) and the inner radius R of the coil as the same of the used mould for its construction:

a) In the case of few numbers of turns the thickness δ can be negligible, thus Equation 3.1 may apply,

$$d = N\pi R - \frac{d_1 + d_2}{2} - 2d_3. \tag{3.1}$$

b) Otherwise, for a large number of turns, its thickness δ cannot be negligible and Equation 3.2 apply,

$$d = N\pi\left(R + \left(\frac{N}{2} - 1\right)\delta\right) - \frac{d_1 + d_2}{2} - 2d_3. \tag{3.2}$$

In both cases, the total length of the tape to be considered is given by,

$$L = 2d + 2d_1 + d_2 + 4d_3. \tag{3.3}$$

iii. After the cut, insulation with Kapton tape is applied, with the exception of distances d_1 as shown in Figure 3.1 c), which serves to apply the solder material;

iv. The tape is wound to build the desired number of turns. In the case of an odd number of turns, the joint is formed opposite to the middle section of length d_2, otherwise, it will overlap the middle section for an even number of turns. Either case, the extremities of length d_1 are soldered as shown in Figures 3.1 d) and 3.2 (b) to build the short-circuited coil.

The manufacturing process described above is sequentially illustrated in Figure 3.1 and taken as a guideline for the work developed in the present thesis.

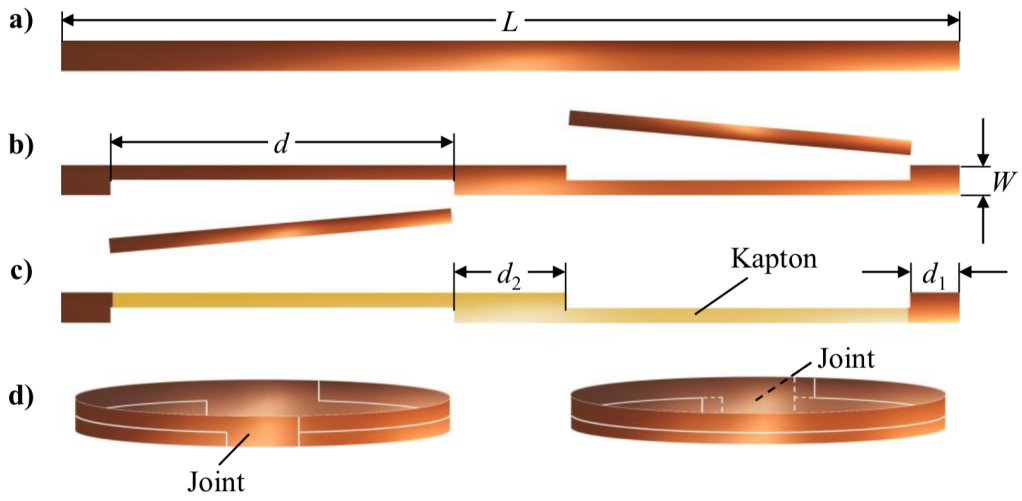

Figure 3.1: Required procedures to implement a short-circuited low-resistance coil with multiple turns. Taken from Murta-Pina et al. (2018).

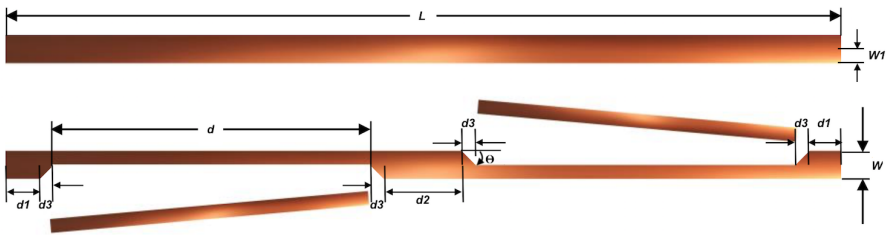

(a)

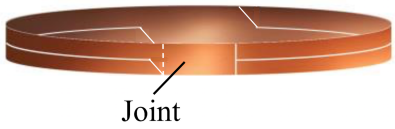

(b)

Figure 3.2: Design of the proposed coil geometry. Adapted from Murta-Pina et al. (2018): (a) The original tape and after the cut (top); (b) Coil built with the proposed design (bottom).

In order to evaluate the degradation that meanders introduce in current density, a meander cut angle θ below 90° is considered for this design for two reasons:

i. To ease the cut through both cut processes considered for this work. Since its more difficult to achieve a right angle, at least in one cut method;

ii. To smooth the meanders corners. Considering an already tested parameter of 30° by Goldacker et al. (2014), used as cross-over angle and to smooth the outer edges of strands in Roeble cables and allow the reduction of von Mises[1] stresses under tensile loads.

Table 3.1: General parameters considered for the design of HTS coils.

General Coil Design Parameters	
The inner diameter of the coil	D
The inner radius of the coil	R
The required number of turns	N
Insulation thickness (Kapton tape)	≈ 0.07 mm
Tape thickness of commercially available CC	0.1 mm
Tape plus insulation thickness, δ	0.17 mm
Length of the slices to be removed from the original tape	d
Distance of the extremities to be soldered	d_1
Distance of the middle section	d_2
Meander cut angle	θ
Original tape width	W
Tape width in longitudinal cut section, W_1	$W_1 = W/2 = A\sin(\theta)$
Meander section, A	$A = W_1/\sin(\theta)$
Meander distance excluded from slices d, d_3	$d_3 = A\cos(\theta)$

[1] The von Mises stress value is mostly used for ductile materials, such as metals, allowing to determine if a material will yield or fracture.

3.2 Cut of the Tapes

Two methods were considered for this work, in order to cut the tapes in the proposed design without damaging its superconducting properties. Namely, water jet and punching. These techniques are detailed in the next sections.

3.2.1 Cut of the Tapes by an Electrician Scissor

This method was not executed in the present work but in Murta-Pina et al. (2018) earlier. Nevertheless, owing to achieved results by this method and the relationship with current work, is important to highlight here the parameters used for the piece of tape considered to build the HTS coil, shown in Table 3.2.

Table 3.2: Considered coil design parameters used for the cut of tapes by a regular stainless-steel electrician scissor. Taken from Murta-Pina et al. (2018).

Coil design parameters for the cut by an electrician scissor	
The inner radius of the coil, R	41.25 mm
The required number of turns, N	3
The total length of the tape, L	803 mm
Length of the slices to be removed from the original tape, d	364 mm
Distance of the extremities to be soldered, d_1	25 mm
Distance of the middle section, d_2	25 mm

3.2.2 Cut of the Tapes by Water jet Method

Water jet cut technology is known as a cold cutting process, i.e., a supersonic erosion process, using supersonic water to cut soft materials (e.g., foam and plastic) or water and abrasive to cut hard materials (e.g., ceramic, metals, glass, composite and stone).

According to Flow International Corporation (2018), it works in three steps:

i. Generate pressure. An ultra-high pressure pump generates a stream of water with pressure rated up to 6480 bar[2] (648 Mpa);

ii. Convert pressure into velocity. The pressure is converted into velocity via a tiny jewel orifice, creating a stream as small as a human hair which can cut soft materials;

iii. Introduce garnet[3] grits as an abrasive. To increase cutting power by 1000 times, garnet is pulled into the supersonic water jet stream. Water and garnet exit the cutting head at nearly four times the speed of sound, capable of cutting steel over 30 cm thick.

[2]Note that: 1 bar = 10^5 Pascal, i.e., 0.1 MPa.

[3]Garnet is used for several applications in the industry owing to its hardness and mineral composition. For the water jet cut, an 80 mesh calibrated sand was used, i.e., grit diameters of $\approx$ 180 microns, typically.

Figure 3.3 illustrates in (a) the mixing process of water and abrasive in a water jet machine cutting head, described above. In (b) the water jet cutting head with 0.33 mm diameter orifice from the Flow Mach 3 4020b machine used to execute this process at 4x4 Multitrabalhos enterprise in Setúbal, Portugal. In (c) the garnet, i.e., an 80 mesh calibrated sand, used as an abrasive in the cutting process.

(a) (b) (c)

Figure 3.3: A water jet cutting head used in the process to cut the tapes: (a) Illustration of a water jet cutting head with the entries for the water and abrasive (left), adapted from Flow International Corporation (2018); (b) The water jet cutting head used in the cutting process (centre); (c) The garnet used as an abrasive (right).

To cut tapes through this method, the pressure was limited in the machine through *Flow Cut* software control to 450 MPa. Additionally, due to the thickness of the tapes (less than 0.1 mm) and the impossibility to steady secure it in the machine, it was necessary to sandwich the tapes between acrylic and wood materials. With this process, a range of 7-12 mm total thickness was obtained, and Figure 3.4 shows this process.

Figure 3.4: A tape sandwiched between the acrylic and wood materials to allow the cut process.

To test the method three pieces of tape with a total length of 400 mm were cut varying the velocity of the cut machine, as shown in Figure 3.5. The velocity is automatically adjusted by the software module based on the specified imperfection margin, i.e., the lower the specified imperfection margin, the higher the velocity of cut.

The water jet actuates from top to the bottom, therefore, e.g., an imperfection margin of 40% means that from the top, 60% of the material is cut to an optimum finish and the rest to a more rough finish.

Figure 3.5 shows the result of three cuts varying two parameters, namely the total thickness and the imperfection margin in the software module of the machine. Firstly 7 mm with 40% (tape at the bottom), second 7 mm with 20% (tape in the middle) and last 12 mm with 20% (tape on top) which provided a better result.

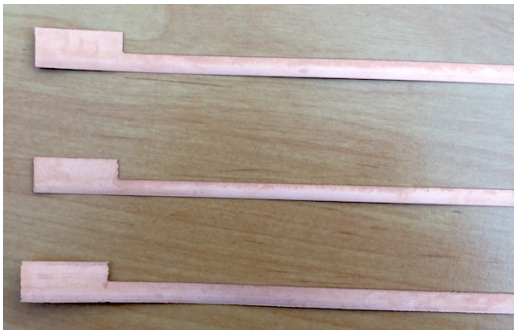

(a)

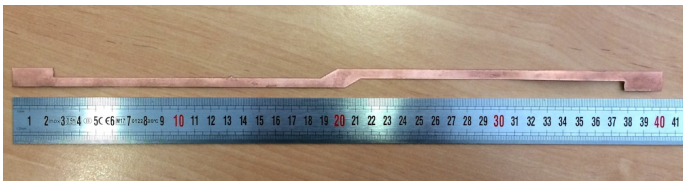

(b)

Figure 3.5: Three tape pieces of 400 mm cut by the water jet to test the method: (a) A zoom for one of the extremities; (b) An overview of the combined mixed geometry with the extremities as illustrated in Figure 3.1 b) and middle section as illustrated in Figure 3.2 a).

Tested the water jet cut process, the cutting machine parameters were set for 12 mm of total thickness with 20% of imperfection margin. Two tapes were cut according to the design illustrated in Figure 3.2 (a) and the parameters specified in Table 3.3, in order to obtain the tapes for four and eight turns, respectively.

Table 3.3: Calculated design parameters for two tapes, to build coils with four and eight turns considering the thickness δ introduced by the Kapton tape.

Calculated design parameters for two tapes cut by water jet		
The required number of turns, N	$N = 4$	$N = 8$
Total length of the tape, L	1072 mm	2137 mm
Length of the slices to be removed from the original tape, d	478 mm	1010 mm
Distance of the extremities to be soldered, d_1	25 mm	25 mm
Distance of the middle section, d_2	25 mm	25 mm
Meander distance excluded from slices d, d_3	10.4 mm	10.4 mm

The parameters indicated in Table 3.3 will also be used to cut tapes using the punching method, presented in section 3.2.3.

Figure 3.6 shows the result of a 1072 mm long piece of tape, cut by water jet to build a coil with four turns.

Figure 3.6: Result of a 1072 mm long piece of tape cut by water jet.

- ***Water jet cutting issues***

The machine used in the water jet cutting process is a conventional machine employed to cut different materials. Consequently, the cut process has to be adapted in order to cut the tapes with longer lengths due to tank limitations and fixation of the tapes.

Figure 3.7 shows in (a) the process and difficulty to fix a 2-meter length tape inside the machine tank to proceed with the cut, therefore, for longer lengths, it turns out to be impracticable. In (b) a zooming area showing the roughness of the edge of tape after the cut.

(a) (b)

Figure 3.7: The issues on using the water jet cut method: (a) The fixing process of 2137 mm tape in the machine tank for the cut; (b) The roughness of the edge of the tape after the cut.

Figure 3.8 shows delamination caused on tapes after the cut by this method, in (a) the tape used to build the coil with 4 turns, and in (b) the three 400 mm pieces of tape cut in the first place to test the method and adjust the parameters to use next.

(a) (b)

Figure 3.8: Delamination issues due to the utilization of water jet cut method: (a) Delamination in one of the extremities of the tape designed for a coil with 4 turns; (b) Roughness of the edges and delamination in the 3 pieces of tape firstly tested.

In summary, even with the pressure limited into the water jet machine at 450 MPa and considering the estimated ultimate tensile strength[4] supported by the acrylic in 70 MPa, the applied transverse tensile is way above the 100 MPa supported by the tape as seen in section 2.3.2. Therefore, this can contribute to premature degradation of the tape.

3.2.3 Cut of the Tapes by Punching Method

This method as described in section 2.4.2 uses a fast real-to-real computer-controlled pneumatic punching tool with a 60 kNm^{-2} pneumatic press shown in Figure 3.9.

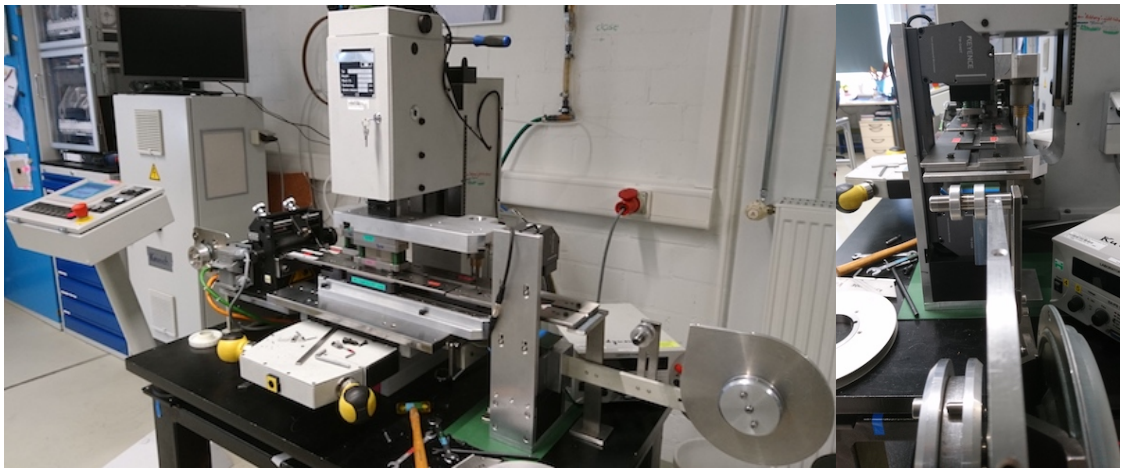

(a) (b)

Figure 3.9: An overview of the punching machine used to cut the tapes through the punching method. Images courtesy from Drs. Wescley de Sousa and Anna Kario, ITEP/KIT: (a) The real-to-real punching machine used; (b) Lateral view of the punching machine.

[4]Ultimate Tensile Strength (UTS) is defined as the limit stress at which the material actually breaks, with a sudden release of the stored elastic energy.

The system is constituted by a roller feeder for tapes and a combination of two movable punches and dies (back and front) as shown in Figure 3.10.

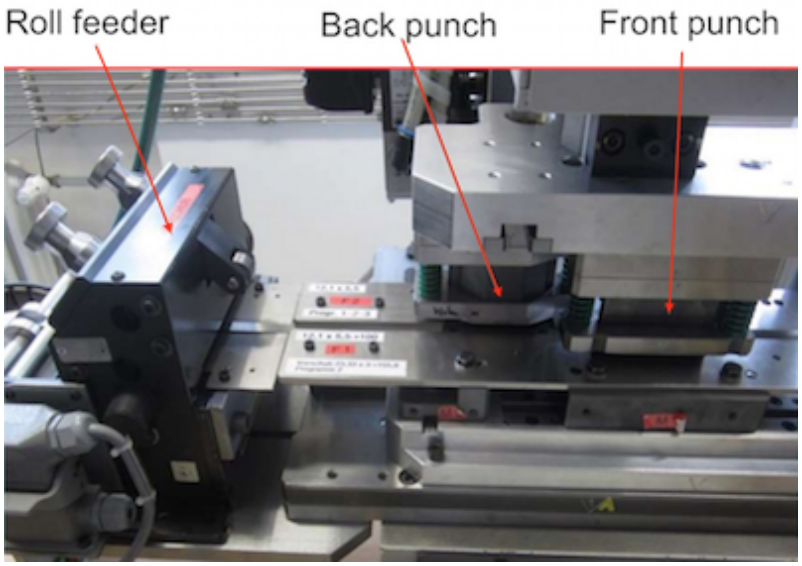

Figure 3.10: Pneumatic adjustable punching tool. Adapted from Goldacker et al. (2016).

This specifically designed punching tool provides a cutting edge with high precision where only the copper is smeared along the cut. It is a more mature technique for this purpose and permits a favourable finish, considering the cut result at the REBCO layer with acceptable uniformity and no drifts of the cut dimensions.

As an advantage, this technique has the flexibility to cut by punching in different geometries owing to its movable punches. However, multiple steps per transposition are needed in case of repeated transitions, e.g., in Roeble cables.

Figure 3.11 shows a zooming area of the transition section of a tape cut by this method according to the geometry illustrated in Figure 3.2. This processed was executed at KIT in Karlsruhe, Germany.

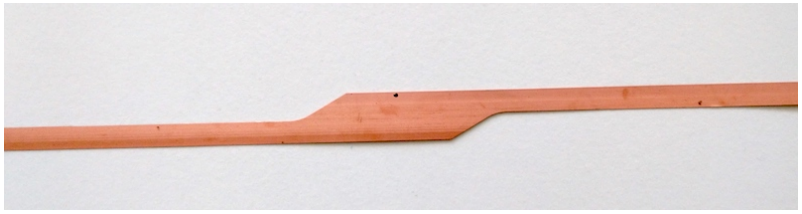

Figure 3.11: Zooming area of a transition section for a 1072 mm tape cut by the punching method.

A piece of tape considered to build a coil with four turns was cut by this method, resulting in a smoother cutting edge and no delamination was observed after the cut.

3.3 Determination of Critical Current

The tapes were cut by the two described methods, namely, water jet and punching. Therefore, it is essential to assess the degradation in its critical current density after the cut processes. Again, due to the relationship with this work, is important to highlight here the critical current density measured values for a piece of tape cut by an electrician scissor, as mentioned above in section 3.2.1.

To a better understanding of these measured values, Figure 3.12 shows a representation for the considered points of measure in the different tapes after the cut, in order to measure the following parameters:

i. The critical current I_{c1} in a straight section, degraded (after cutting);

ii. The critical current I_{c2} considering the meanders effects, in the transition section.

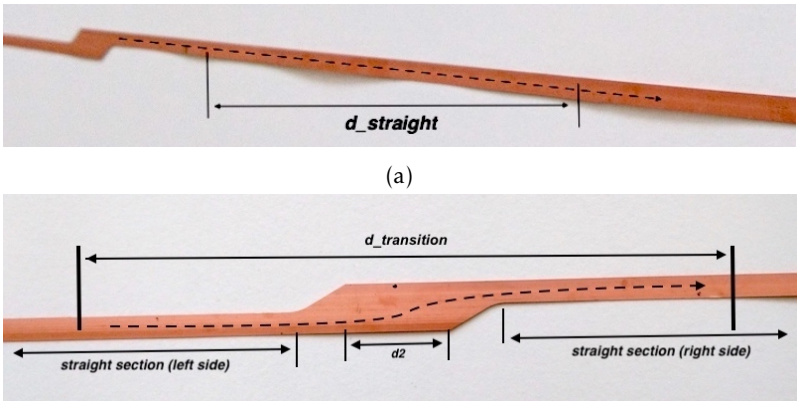

(a)

(b)

Figure 3.12: Considered points for the measurement of I_c current on the tapes: (a) Straight section on the tapes with 6 mm width after the cut to measure I_{c1}; (b) Transition section to assess the effect of the meanders on the I_{c2} current.

Table 3.4 shows three measured values of critical current for further comparison of the methods. I_{c0} from the original tape which is aligned with a specified value from the manufacturer, I_{c1} after the cut with design illustrated in 3.1 b) considering a section in the distance d and I_{c2} with the effect of the meander including the distance d_2.

Table 3.4: Measured values of critical current for the cut by a regular stainless-steel electrician scissor. Taken from Murta-Pina et al. (2018).

Values of critical current for the cut by an electrician scissor	
Critical current of the tape prior to cutting, I_{c0}	362.5 A
Critical current of the tape after cutting, I_{c1}	178.7 A
Critical current due to the meander, I_{c2}	166.6 A

Using the $E-J$ power law given by Equation 3.4, to describe the characteristic curves near the transition between the superconducting and normal conduction. The criterion of $E_c = 1\mu V/cm$ for 2G HTS, to define the critical current, due to a not well-defined transition in the electric field. It is possible to determine experimentally the critical current on the tapes through distances considered in Figure 3.12.

$$E = E_c\left(\frac{J}{J_c}\right)^n, \tag{3.4}$$

where E_c represents the critical electric field, J_c the critical current density on the tape and n value represents the shape of $E-J$ curve which characterizes the transition between normal and superconducting states, in this case, with its values assessed by a fitting tool.

Since it is more practical to measure the voltage and current than the electric field and the current density, the law is adapted for voltages corresponding to the critical currents.

Therefore, knowing that, for a uniform field the electric field can be expressed by $E = U/d$, where U is the voltage between two measure points and d is the distance between them. Analogously, the current density can also be expressed by $J = I/A$, where I is the amount of electric current that flows per unit area A of the material cross-section. Thus, replacing these two quantities in Equation 3.4, the relationship is then given by Equation 3.5.

$$U = U_c\left(\frac{I}{I_c}\right)^n. \tag{3.5}$$

The critical current I_c is determined by the point of intersection between the curve that represents the experimental points and the line representing the given critical voltage between the measuring points. The critical voltage line is expressed by Equation 3.6.

$$U_c = E_c \cdot d, \tag{3.6}$$

where for a straight section as in Figure 3.12 (a) the distance $d = d_{straight}$, otherwise, for the transition section as in Figure 3.12 (b) the middle line distance represented on tape is $d = d_{transition}$ which can be approximated by the expression:

$$d_{transition} = l - d_2 + \frac{d_2}{\cos(\theta)}, \tag{3.7}$$

where l is the considered distance between two points of measure, d_2 and θ are the distance for the transition section and the angle for meander, respectively, parameters presented in Table 3.1 and illustrated in Figure 3.2 (a).

Figure 3.13 shows an example of an assembly for the critical current measurements on the tapes, designed and cut by both methods to build coils with four turns. In (a) a tape cut by water jet dipped in liquid nitrogen during the measurements. In (b) an assembly

to measure the critical current in both considered sections, straight and transition, before the dip in the liquid nitrogen, for a tape cut by punching. This process needs to be carefully executed to avoid damages on the tapes.

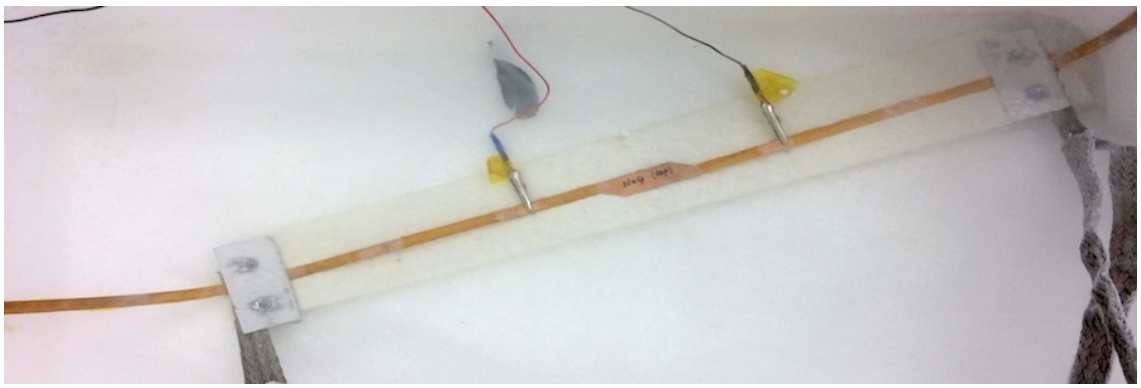

(a)

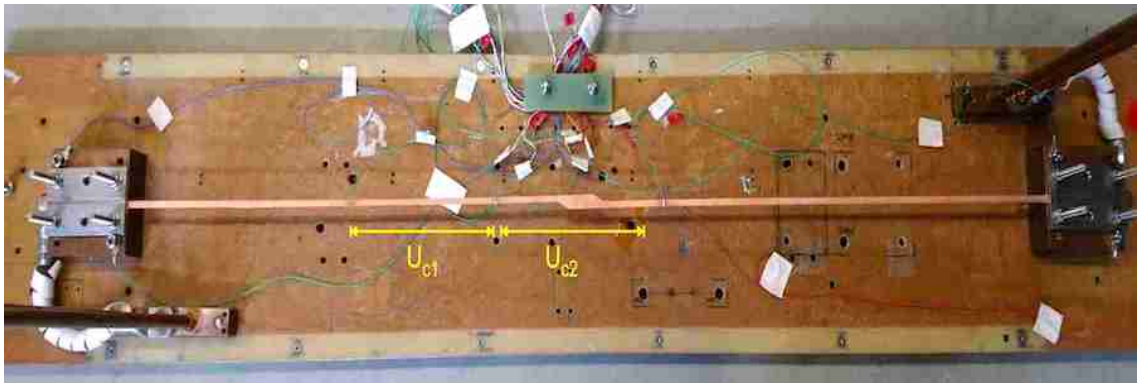

(b)

Figure 3.13: Examples of experimental assembly for measurements of critical currents I_c on 1072 mm length tapes: (a) For a tape cut by the water jet method; (b) For a tape cut by the punching method.

Figure 3.14 shows one of the issues that can occur in case of excess current injected into the tapes, i.e., above the supported critical current of the tape in that section.

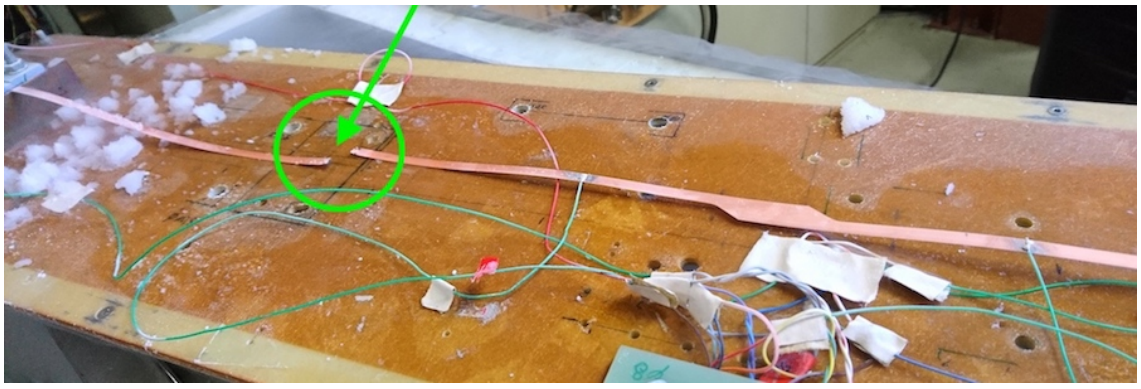

Figure 3.14: Rupture of tape due to excessive injected current.

3.3.1 Critical Current after Water Jet Cut

Next, the results of measured critical current using the four-points method are presented for the first three tapes tested by the water jet cutting method, along with the two tapes cut by the same method to build the HTS coils.

- ***First three tapes tested, cut by the water jet***

Test results for the first tape, cut by water jet, are shown in Figure 3.15. After three tests, the critical current I_{c1} in the straight section was measured between 74-76 A as shown in (a), where the curve shape for the measured points has a step of transition from superconducting to normal conduction at E_c described by the power factor $n = 16$. Whereas, in the transition section, measured critical current I_{c2} was between 89-93 A as shown in (b), with an n value of 13.

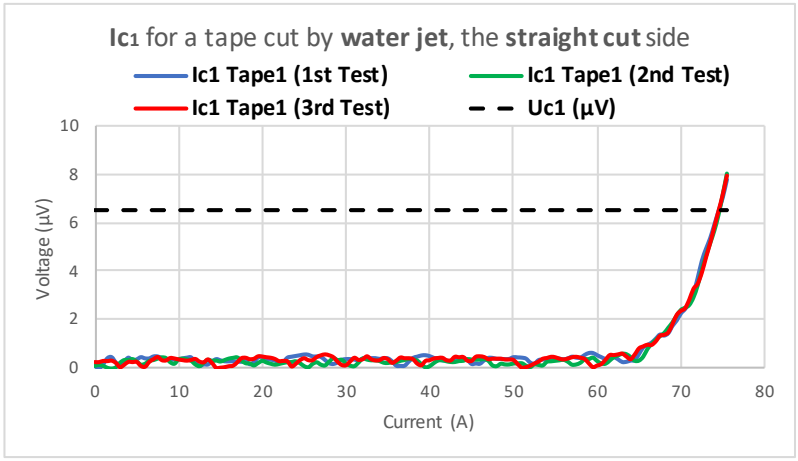

(a)

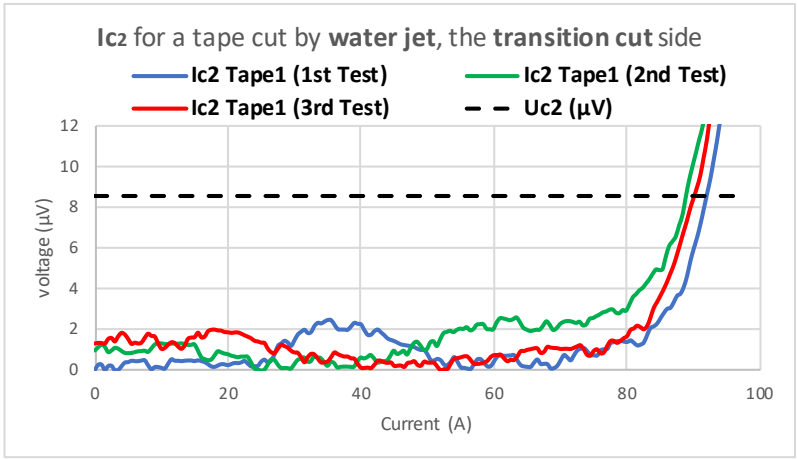

(b)

Figure 3.15: Results of Ic critical current for the first of three tested tapes: (a) The I_{c1} current for the straight section; (b) The I_{c2} current for the transition section.

For the second tape, three tests were executed again as shown in Figure 3.16. Here, the emphasis was on the effect introduced by meanders in current density and on improving the cut process by this method. Thus, measured critical current I_{c2} for the transition section was around 108.5 A and the curve shape described by an n value of 15.

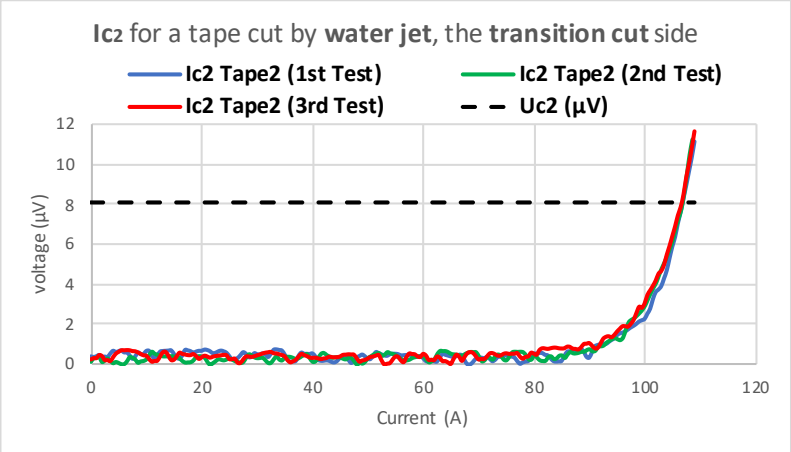

Figure 3.16: Results of Ic critical current for the second of three tested tapes: The I_{c2} current for the transition section.

For the third tape, three tests were also executed and Figure 3.17 shows measured critical current I_{c2} for the transition section around 128 A and the curve shape described by the power factor $n = 15$.

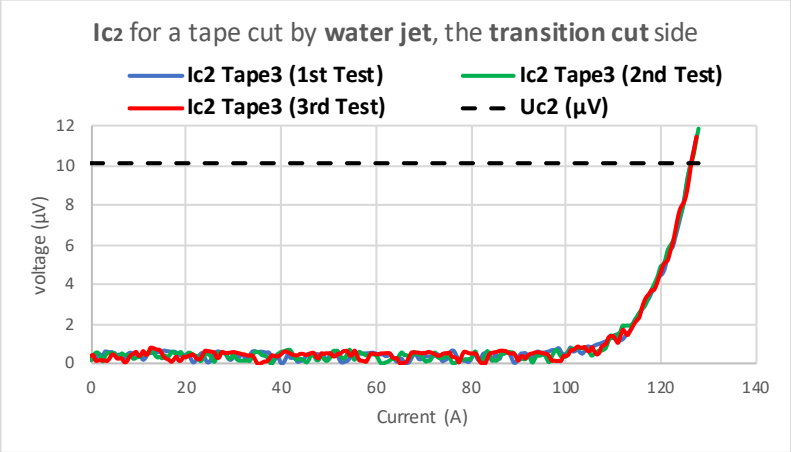

Figure 3.17: Results of Ic critical current for the third of three tested tapes: The I_{c2} current for the transition section.

The difference between results, where an increase of the critical current is observed from first to the third tape in the transition section, is explained in part by the cut process, which was enhanced by reducing the water jet velocity and limiting the pressure at 450 MPa to cut the tapes sandwiched. In addition, the n values were assessed considering the power law.

There is a discrepancy in the literature between the n values measured by different experimental techniques for commercially available YBCO conductors as the ones used in this work. However, n values close to 21 measured under self-field conditions at 77 K are reported as a good fit for HTS by Vanderbemden et al. (2007) and adopted by many authors. Although, under the same measurement conditions, values between 30 and 45 are also reported for the same type of conductors with 4 mm width, according to Tsuchiya et al. (2017).

- ***Tapes for four and eight turns, cut by the water jet***

Figures 3.18 and 3.19 show the results for the tape used to build the coil with four turns. The values of I_{c1} critical current differ from left straight section to the right, with values of 135 A and 129 A, respectively. This difference can be explained by the degradation of the edges through the cutting process.

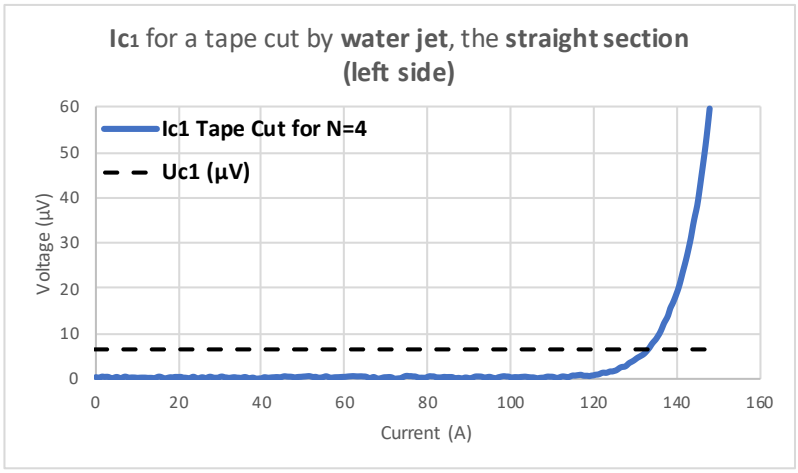

(a)

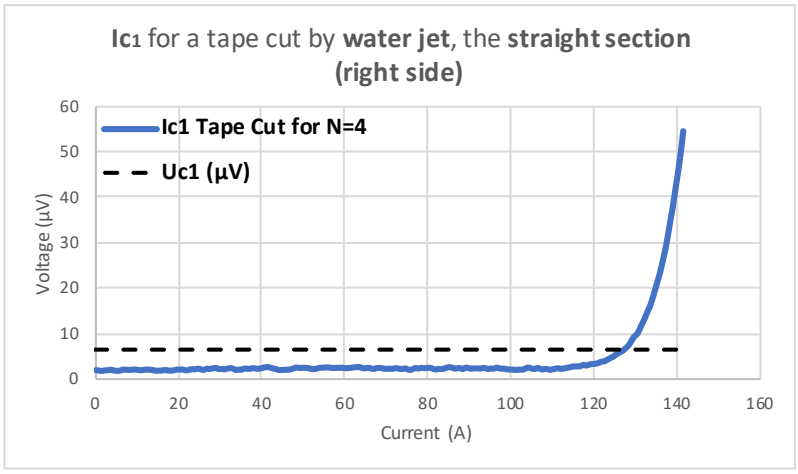

(b)

Figure 3.18: Results of Ic critical current for the N4 tape, cut by water jet: (a) The I_{c1} current for the left straight section; (b) The I_{c1} current for the right straight section.

The I_{c2} critical current at transition section is higher, i.e., 138 A, than those obtained for the straight section. Considering that meanders introduce degradation in the current density, it means that the degradation of cut edges in the tape for the straight section is considerable. The curve shapes for these three sections are assessed by an n value of 20.

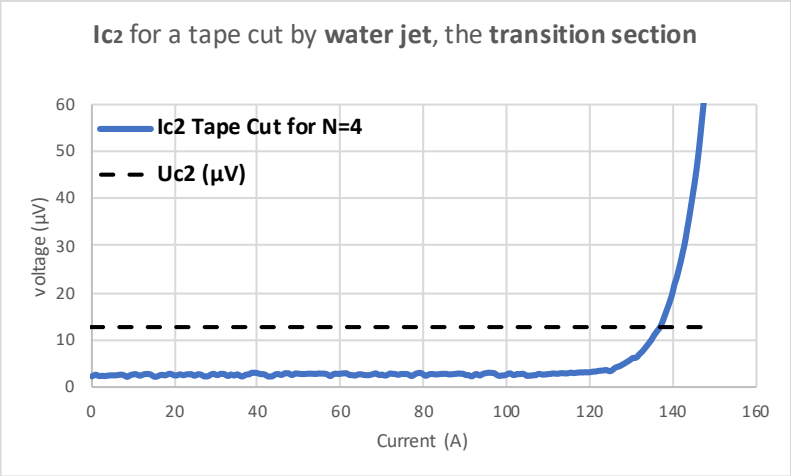

Figure 3.19: Results of I_{c2} critical current for the N4 tape cut by water jet, at transition section.

The tape considered to build the coil with eight turns did not end up with both straight sections with the same width. It was due to the difficulty in aligning the tape along the machine tank for the cutting process, as illustrated in Figure 3.7 of the section 3.2.2. Therefore, it had an impact on the measured results for the I_c critical current as shown in Figures 3.20 and 3.21.

Two tests were realized for the left straight section (the thinner side) and one for the right straight section (the thicker). The results show a huge difference between the two sides, with 39 A and 119 A for the I_{c1} critical current, thin and thick sides respectively.

The result in the transition section is different from expected, i.e., between 23-24 A for the I_{c2} critical current, when compared with the tape for four-turns and cut by the same method. This situation can be explained again, by the degradation of the edges through the cutting process and the delamination verified for certain sections of the tape after the cut, which clearly affected the superconducting properties of the tape and resulted in a non-homogeneous conductor.

The curve shapes for these three sections were also assessed, being for the left straight section $n = 11$. Whereas, for the right straight section, it was not possible to assess the n value using the same fitting tool due to the quality of measured points. For the transition section, the curve shapes are described by an n value of 9.

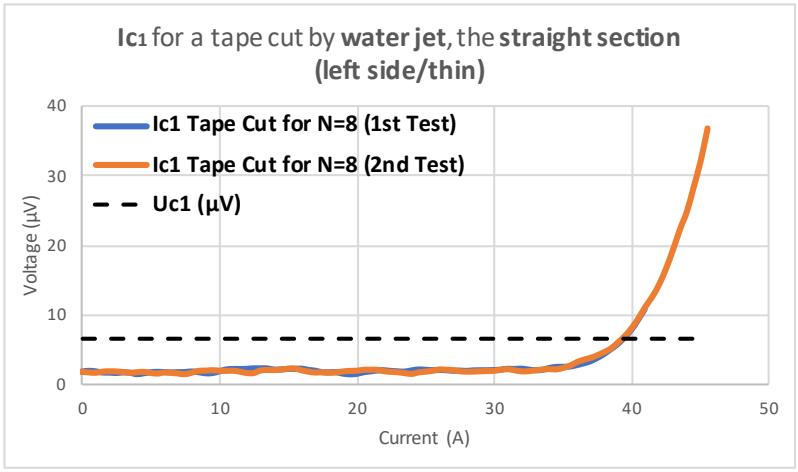

(a)

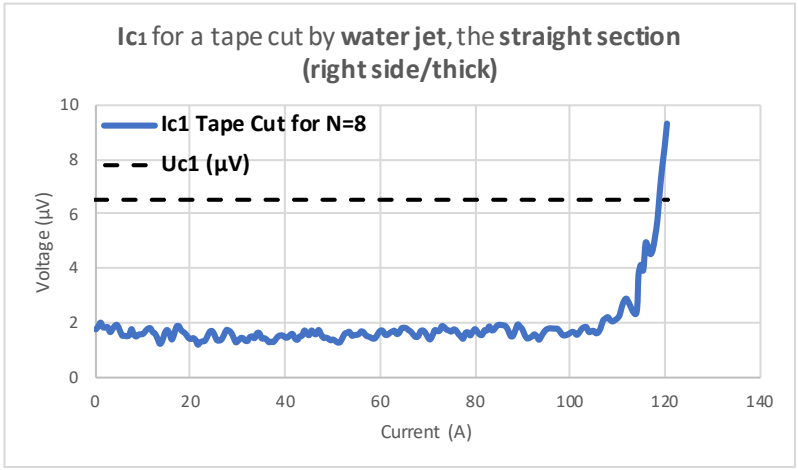

(b)

Figure 3.20: Results of Ic critical current for the N8 tape, cut by water jet: (a) The I_{c1} current for the left straight section (thin side); (b) The I_{c1} current for the right straight section (thick side).

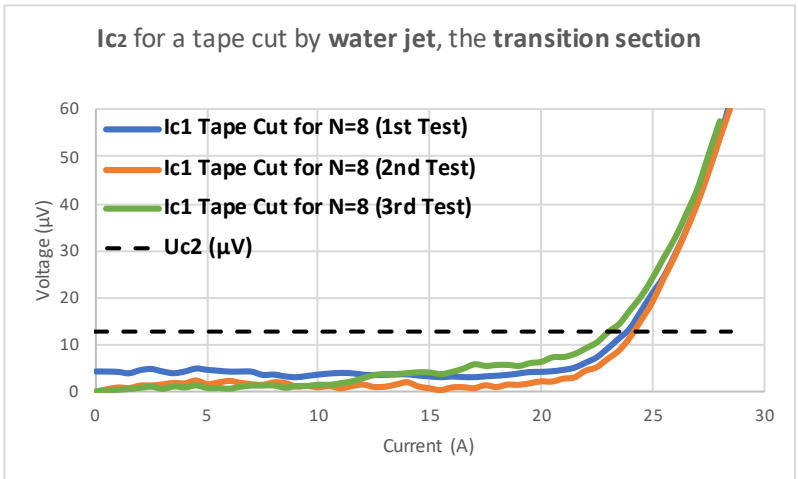

Figure 3.21: Results of I_{c2} critical current for the N8 tape cut by water jet, at transition section.

3.3.2 Critical Current after Punching Cut

The results of measured critical current for a tape cut by the punching method and intended to build a coil with four turns are presented in this section.

- ***Tapes for four turns, cut by punching***

The punching method led to better results in comparison with those obtained from the water jet method. This can be explained by the used cut technique which revealed less harmful for the edges of the tape after the cut, preserving the contact surface of the tapes and providing an optimal finish for the edges and preventing its delamination.

Figure 3.22 shows measured results for the critical currents at straight and transition sections, 177 A for I_{c1} and 165 A for I_{c2}, respectively. Confirming the degradation of critical current due to the effect of meanders. The curve shapes were also assessed, being the power factor n of 26 and 27 for the same sections, respectively.

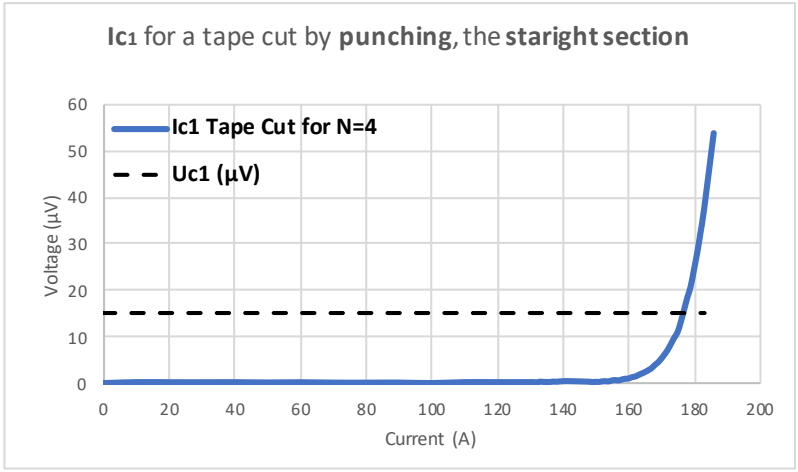

(a)

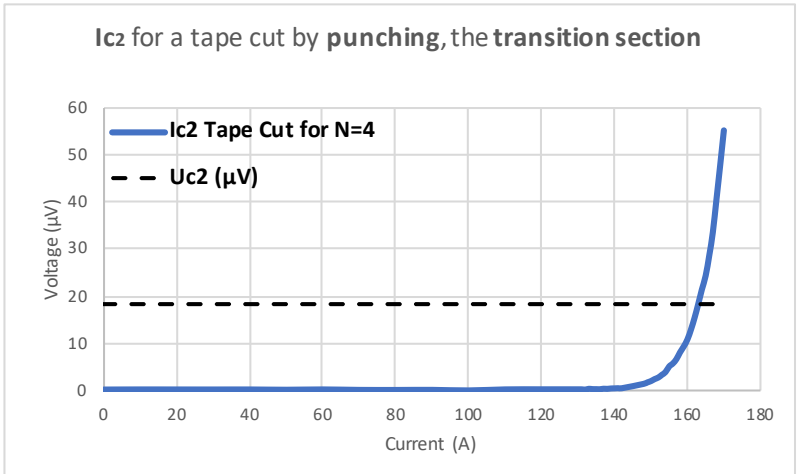

(b)

Figure 3.22: Results of Ic critical current for the N4 tape, cut by punching: (a) The I_{c1} results for the straight section; (b) The I_{c2} results for the transition section.

3.3.3 Comparison of the Cut Methods

Table 3.5 summarize measured results for the critical currents on different tapes considered in the present work. Emphasis goes for the punching method which allowed higher critical current values when compared to water jet method. Nevertheless, the previous results measured by Murta-Pina et al. (2018) and indicated in Table 3.4 are aligned with the results from the punching method measured in this work. Therefore, two important conclusions to retain:

i. The water jet method reveals more aggressive for the cut purpose, less precise and difficult to handle when comparing to the punching method;

ii. Each of the tested cut methods degrades the critical current of the tapes mainly in the meanders.

Table 3.5: Summary of I_c critical current measurements for different tapes.

Measurement results of the Ic current for the different tapes cut								
Cut method	Tape	d_2 [cm]	$d_{straight}$ (left) [cm]	I_{c1} [A]	$d_{transition}$ [cm]	I_{c2} [A]	$d_{straight}$ (right) [cm]	I_{c1} [A]
Water jet	**tape1**	0.5	6.5	74-76	8.58	89-93	–	–
	tape2	0.5	6.5	–	8.08	108.5	–	–
	tape3	0.5	6.5	–	8.58	128	–	–
	tapeN4	2.5	6.5	135	12.89	138	6.5	129
	tapeN8	2.5	6.5	39	12.89	23-24	6.5	119
Punching	**tapeN4**	2.5	15	177	18.39	165	–	–
Electrician scissor		2.5	–	–	8.6	166.6	3	178.7

Note: Values from the previous prototype with the tape cut by a regular stainless-steel electrician scissor was taken with permission from Murta-Pina et al. (2018).

3.4 Synopsis

This chapter presented the design of tapes considered to build HTS coils, explaining the architecture and the design process.

The two processes used to cut the tapes were detailed, indicating the advantages and constraints for each one.

The methodology used to determine the critical current on the tapes was addressed and the measured results presented and discussed.

Finally, a comparison of the cut methods was done.

4 | Analysis of Joining Process

This chapter presents the determination of the joining process to be used in the prototypes. Experimental procedures concerning the joining of the tapes are addressed and measurements of normal (non-superconducting) resistances for different considered joints are presented and discussed.

4.1 Experimental Procedure for the joints

To define which solder material and topology to use in the joining process of the coils is necessary to determine the contact resistance of the joints because these are points of ohmic losses which must be minimized.

First, several linear joints with different solder materials and configurations were built, i.e., in lap and bridge topologies. Next, the resistance for each joint at cryogenic temperature (dipped in liquid nitrogen) was measured through the four-points method illustrated in the schematic of Figure 4.1.

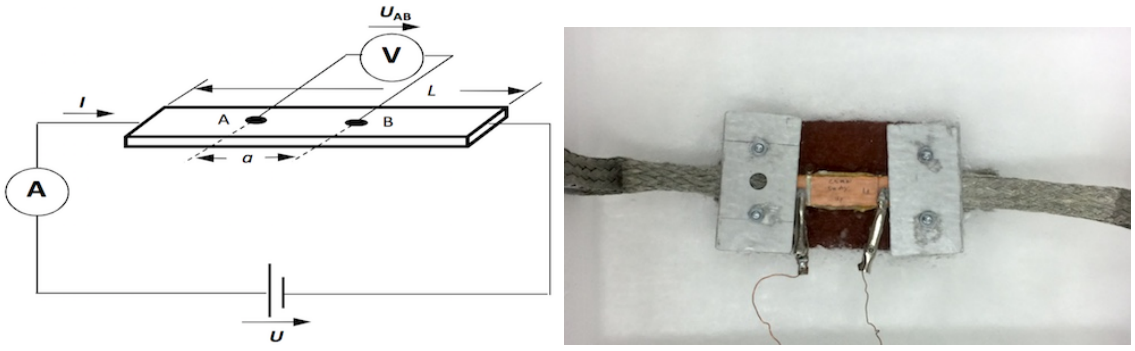

(a) (b)

Figure 4.1: Measuring example for the contact resistance of the joints by the four-points method: (a) Schematic of the four-points method used to measure the joint resistance. Taken from Pronto (2010); (b) A joint made with SnAg paste using the lap topology, dipped in liquid nitrogen to measure the contact resistance.

Three different solder materials were considered to build the joints, one in ribbon (indium) and two in readily mixed solder pastes (SnAg and SnAgCu). The soldering of

the tapes was carried out in a temperature controlled home electric oven and the relevant information about the soldering time is detailed in Table 4.1.

Table 4.1: Summary of the temperatures and time used to build the linear joints.

Solder paste	Melting point (MP)	Home oven heating time	Time after reaching the MP
In ribbon	157°	30 min	3 min
96.5Sn 3.5Ag	221°	30 min	2 min
96.5Sn 3.0Ag 0.5Cu	220°	30 min	2 min

Following the parameters of temperature and time from Table 4.1 eight linear joints were built, being three in lap topology and four in bridge. Furthermore, joints with solder paste were repeated to enhance the joining process in the bridge topology, considering the third piece needed to build the joint and to guarantee at least one good joint built in this configuration.

Figure 4.2 shows different joints which resulted from this process and the simple device used to build them, exerting the adequate pressure on overlapped pieces of tapes with solder material within.

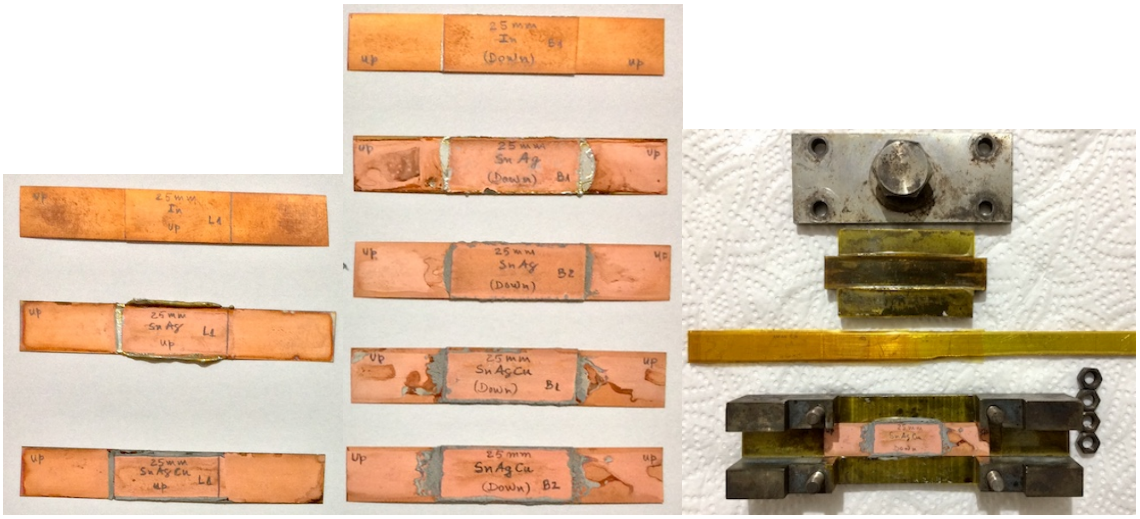

(a) (b) (c)

Figure 4.2: Joints built to determine the contact resistance: (a) Different joints in lap topology; (b) Different joints in bridge topology; (c) Device used to build linear joints in both configurations.

4.2 Determination of the joining method

The resistance of the joints was measured at a cryogenic temperature as illustrated in Figure 4.1. During the measuring process, the indium joint in lap topology opened when trying to fix the joint in the assembly, consequently, it was not possible to determine its contact resistance.

Figure 4.3 shows the opened indium joint. It is important to highlight this issue which can be explained, in part, by the fragility of the achieved joint when this solder material is applied directly to the electroplated copper of the CC, as was done for the others joints containing SnAg and SnAgCu. According to Indium-Corporation (2016), it is not recommended because indium and copper diffuse into one another forming a brittle inter-metallic layer.

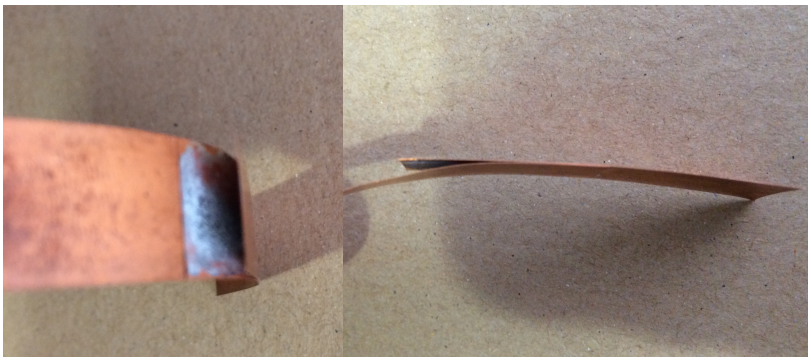

Figure 4.3: Example of a fragile joint when using indium solder material applied directly to electroplated copper.

Figure 4.4 shows a comparison of the different joints made with SnAg solder paste in both topologies and considered for the present work. The measured results show that all joints made with this solder material have very close values for the contact resistance, between 1.74-1.90 $\mu\Omega$, independently from the configuration.

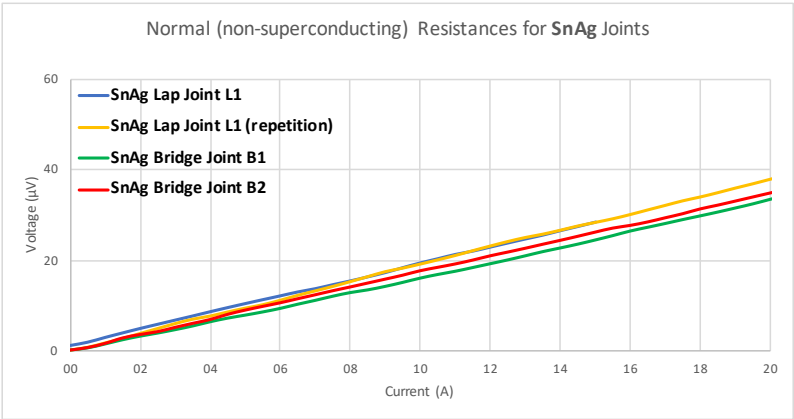

(a)

Figure 4.4: Comparison of different joints built with SnAg solder paste in lap and bridge topology.

For the proposed design, the HTS layer orientation is maintained across the joint. Therefore, for lap topology, the solder is applied between the HTS side and the substrate side of the tape, as shown by the orientation of splices in Figure 4.2 (a), instead of facing each HTS side (in a face-to-face configuration).

Due to exposed reason, significantly higher electrical resistances can occur, since the current must pass through additional layers. Therefore, one of the reasons to explain the results in the order of micro-ohms. In contrast to contact resistances reported by manufacturers in order of 80 nΩ for joints of 25 mm length (AMSC, 2012) or below the 20 nΩ for joints of 100 mm length (SuperPower-Inc., 2014). Duplicating the values when using the bridge topology and same lengths.

Figure 4.5 shows in (a) that lap configuration presents values slightly above than in bridge for the SnAg solder paste on average. Again, this is influenced by the chosen configuration and cannot be discarded the soldering process executed in a conventional home oven or the validity of the solder paste acquired earlier. Comparing the joints made with SnAgCu paste in (b), a lower value is also observed in the bridge configuration.

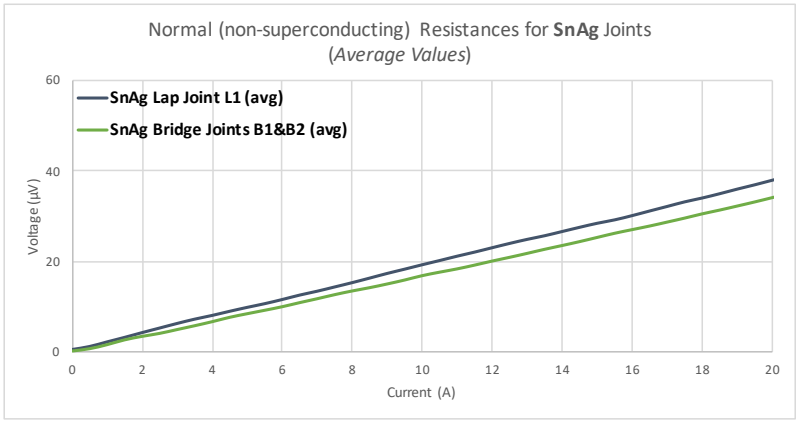

(a)

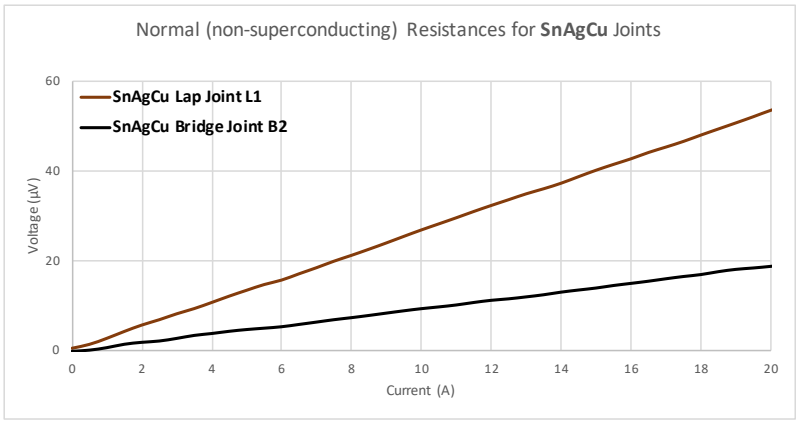

(b)

Figure 4.5: Comparison of different joints built with SnAg and SnAgCu solder pastes: (a) Joints built with SnAg solder paste in both configurations, average values; (b) Joints built with SnAgCu solder paste also in both configurations.

A comparison by the used topology in the different joints is shown in Figure 4.6. In (a) the joints are compared by lap configuration and the result show a lower contact resistance achieved with SnAg solder paste, considering the two joints made with this

soldering material.

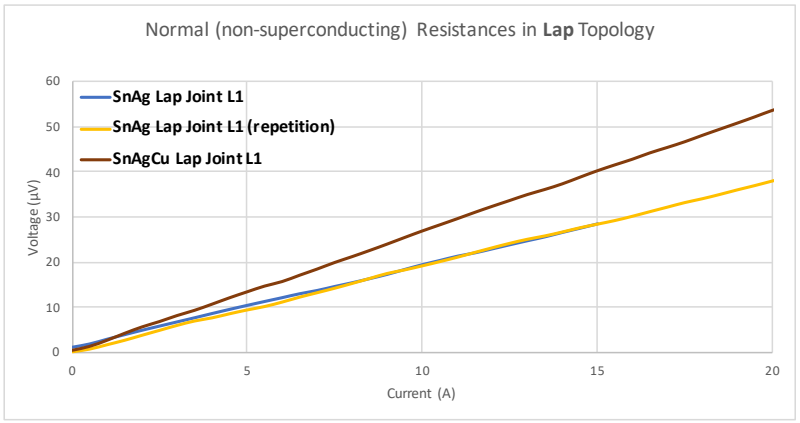

(a)

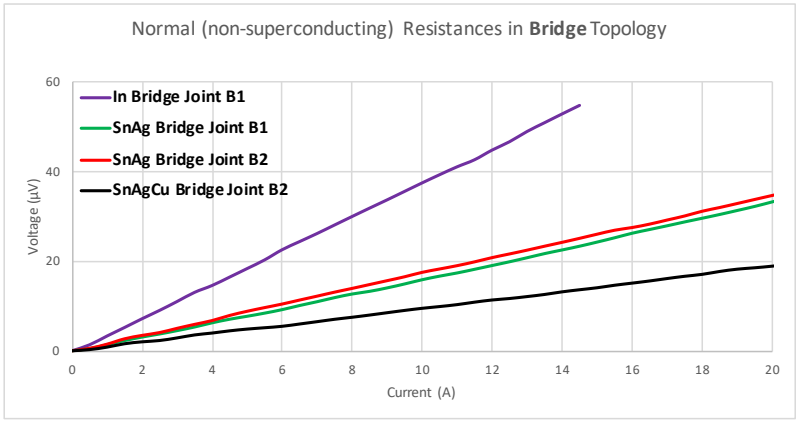

(b)

Figure 4.6: Comparison of different joints by topology: (a) Comparison by lap configuration; (b) Comparison by bridge configuration.

In (b) the result shows that in bridge configuration the worst value is achieved with indium ribbon, influenced by the reaction between the indium and the copper in the tapes as exposed above. For the SnAg solder paste, the two considered joints present very similar values, although slightly above the one presented for the SnAgCu solder paste.

Table 4.2 summarize the normal (non-superconducting) resistance values of the joints measured for the three solder materials used in the work.

Table 4.2: Summary of the normal resistance values of the joints tested.

Normal resistance of the joints for the different solder pastes tested		
	Lap configuration ($\mu\Omega$)	Bridge configuration ($\mu\Omega$)
In (ribbon)	–	3.78
96.5Sn 3.5Ag	1.90	1.76
96.5Sn 3.0Ag 0.5Cu	2.67	0.92

Considering the measured values for the joint resistances summarized in Table 4.2, there are two important results which led to the choice of the solder material and the configuration to use in this case:

i. The normal (non-superconducting) resistance of both joints with SnAg present less variability of the results when comparing the two topologies, despite the lower value achieved with one SnAgCu joint in bridge (the other was not considered due to the extremely high value of 40 $\mu\Omega$);

ii. The fact that the tape designed for four turns presents delamination after the cut process in one of the extremities used to apply the solder material, it is recommended to short-circuit the tape using the lap configuration.

Due to these two reasons, the solder material considered to build the coils with four and eight turns was the SnAg using the lap configuration with 1.9 $\mu\Omega$ of joint resistance and a specific resistivity of 5.7 $\mu\Omega\text{cm}^2$ (1.9 $\mu\Omega$ $\times$ 2.5 cm $\times$ 1.2 cm). The joint resistance is close to 2.15 $\mu\Omega$ for the same contact area and solder material achieved in Murta-Pina et al. (2018).

4.3 Synopsis

This chapter presented the experimental procedure to build different joints in order to measure the contact resistance of the joints.

The measured results for the different joints were presented, discussed and a method to build the joints for the short-circuited HTS coils was defined.

5 Development of Prototype Coils

This chapter will present the specified parameters for the developed prototypes, the experimental procedure to build the HTS coils and the test of these prototypes in order to determine the critical current. The results will be presented and discussed.

5.1 Design of the HTS Coils

In Section 3.1 the design of the coils was exposed and the specified parameters for the prototypes are detailed in Table 5.1.

Table 5.1: Specific parameters for the two prototype coils.

Specified Coils Parameters		
The inner diameter of the coil	83 mm	
The inner radius of the coil	41.5 mm	
Insulation thickness (Kapton tape)	$\approx$ 0.07 mm	
Tape thickness of commercially available CC	0.1 mm	
Tape plus insulation thickness, δ	0.17 mm	
Distance of the extremities to be soldered, d_1	25 mm	
Distance of the middle section, d_2	25 mm	
Meander cut angle, θ	30°	
Original tape width, W	12 mm	
Tape width in longitudinal cut section, W_1	6 mm	
Meander section, A	12 mm	
Meander distance excluded from slices d, d_3	10.4 mm	
Calculated lengths for the two prototypes		
Number of turns, N	$N = 4$	$N = 8$
Calculated distance, d	478 mm	1010 mm
Total length of the tape, L	1072 mm	2137 mm

Table 5.1 shows also calculated values for the distance d and total length tape L, for the 4 and 8 turn coils. These values take into consideration the additional thickness of the Kapton tape contemplated by Equation 3.2.

The distances d_1 at the extremities of the tape use the minimum value for the joint length of 25 mm, recommend by manufacturers like AMSC (2012) and SuperPower-Inc. (2014), which is also the considered minimum bend diameter at joints using the CC of *SuperPower* manufacturer, i.e., the ones used in the present work (2G HTS wire type, reference $SCS12050$ with surround copper stabilizer).

Regarding the angle, 30° for the meander is used to smooth the corners and facilitate the cut process also, this value has been successfully used in cutting Roeble cables through punching techniques from 12 mm width tapes (Goldacker et al., 2014).

5.2 Developed Prototypes

After the measurement of I_c critical current on tapes, it is necessary to insulate with Kapton tape (which withstands high temperatures) in order to build the coils.

The next step is the construction of the coils using an annular mould as shown in Figure 5.1. Since the mould is more bulky and thicker, it is necessary to let it for more time in the oven to get the desired temperature to melt the solder material. Table 5.2 details the time steps taken in order to accomplish the process.

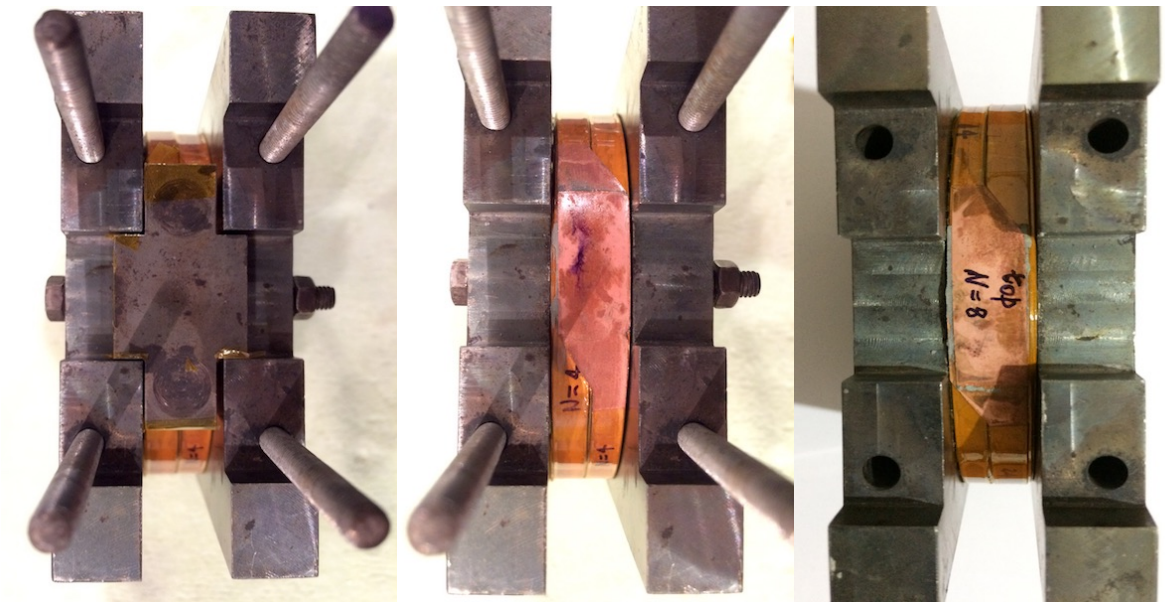

(a) (b) (c)

Figure 5.1: Construction of both coils through the annular mould: (a) The coil with four turns through the assembly mould, before entering the oven; (b) The coil with four turns, after exiting the oven; (c) A coil with eight turns, after exiting the oven.

Figure 5.2 shows the final result with both coils successfully soldered with SnAg solder paste to make the low-resistance short-circuited coils as expected.

Table 5.2: Soldering time steps to build the joints for both coils.

Time steps for the soldering the coils joints	
Oven heating time	35 min
Time to heat the mould and reach the solder melting point	12 min
Time to melt the solder material (SnAg)	2 min

(a) (b)

Figure 5.2: Final result of both prototype coils assembled through the mould: (a) Outer view of the prototypes; (b) Inner view of the prototypes.

Regarding the prototypes, note that they were achieved using the tapes designed for four and eight turns cut by water jet only. Since tape designed for four turns cut by punching method broke during the critical current measurements, as described in Figure 3.14. Consequently, due to the unavailability of the punching cut machine at KIT, it was not possible to execute another cut during the considered period of the present work, in order to assess and compare with the others two prototypes.

5.3 Experimental Procedure

This section has the main objective to measure the critical current in the prototype coils and correlates the results with previous works.

The experimental procedure consists of the induction of superconducting currents in the HTS coils. For this purpose, the prototype coils (as the secondary winding) are concentrically arranged in a 112 turns coil with air core (acting as the primary winding) in order to assess its performance by measuring the critical current it supports.

The electrical diagram of the assembly process is shown in Figure 5.3 and the list of devices is described next:

- An autotransformer 0-400 V (20 A). It allows the application of a variable voltage to the windings of the air-core coil;
- A 112 turns air-core coil, which serves as primary winding to induce currents in the HTS coils through a magnetomotive force;
- Two developed prototype coils, with 4 and 8 turns, concentrically arranged in the air core as illustrated in Figure ;
- Two Rogowski coils (i3000 Flex-24), namely A1 and A2, necessary for the measurement of the currents. This is accomplished by embracing the primary and the air core as illustrated in Figure 5.3. These include the total magnetomotive force provided by the primary, the total current in the superconducting coil and are governed by the equations:

$$\begin{cases} A_2 = i_{Cu} \\ A_1 = N_{Cu} \times i_{Cu} + N_{HTS} \times i_{HTS} \end{cases} \Leftrightarrow \quad i_{HTS} = \frac{A_1 - N_{Cu} \times A_2}{N_{HTS}} \tag{5.1}$$

- One data acquisition *PicoScope* PC oscilloscope, device with signal conditioning and data acquisition board;
- Computer with *PicoScope* software, to perform the necessary readings, recording and data processing of the acquired signals;
- Voltmeter, to control with better precision the variable voltage applied by the autotransformer to copper winding on the primary;
- Ammeter, to measure the maximum current applied on the primary.

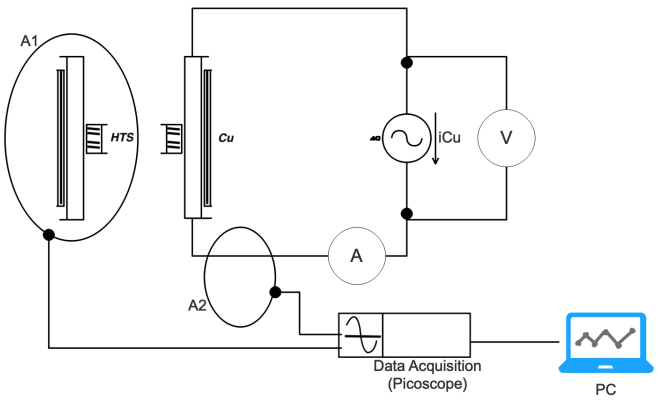

Figure 5.3: Electrical diagram of the assembly process to test the prototypes.

Considering the described assembly, measurements of the critical current at cryogenic temperature were realized at superconductivity laboratory of Faculdade de Ciências e Tecnologia from Universidade NOVA de Lisboa with the apparatus illustrated in Figure 5.4. One of the Rogowski coils is used to measure the current embracing primary winding and the other embrace the primary and secondary windings through the air-core measuring the total magnetomotive force.

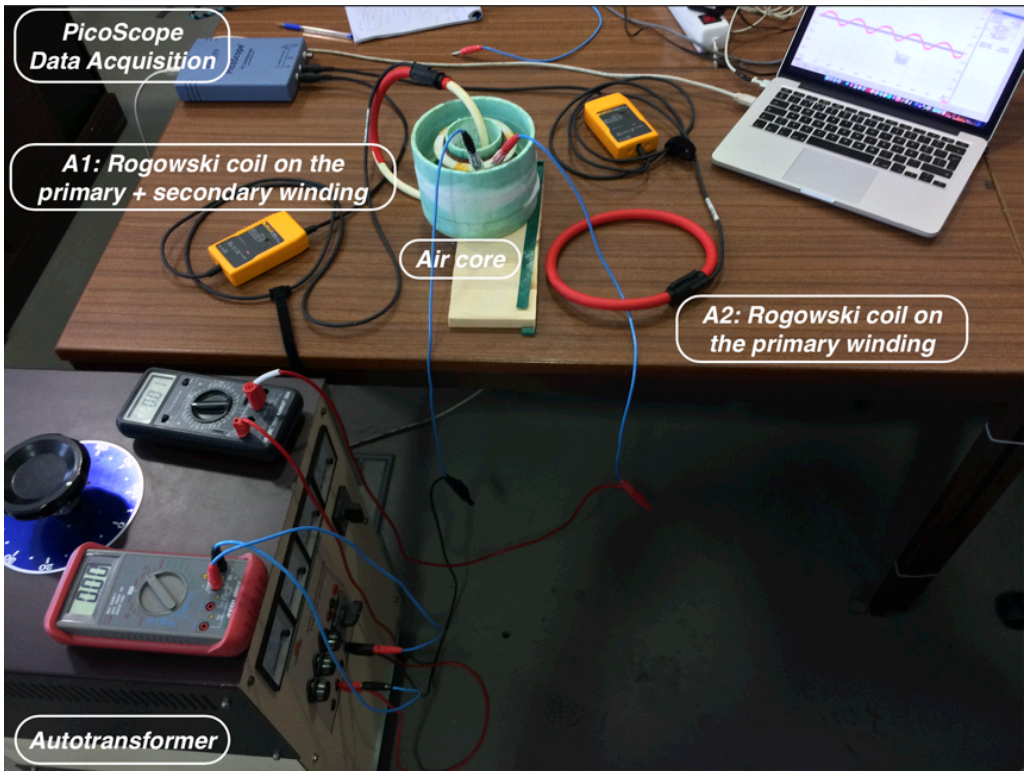

Figure 5.4: Experimental assembly used to measure the currents.

Figure 5.5 shows the arrangement of the air-core with the copper winding and the HTS coils, along with the cryogenic container where the device is dipped in liquid nitrogen.

(a) (b)

Figure 5.5: The 112 turns air-core coil and the cryogenic support: (a) The air-core and HTS coils on the supports; (b) Assembly of the air-core with one prototype coil as secondary winding inserted into the cryogenic container for liquid nitrogen bath.

5.4 Experimental Results and Analysis of the Prototypes

Several points of total magnetomotive force and the current on both windings were measured according to the experimental procedure described in Section 5.3. This section shows these results in order to evaluate the performance of the prototypes.

- ***Results for the prototype coil with four turns***

The voltage was gradually changed in small steps on autotransformer, then for each step values of current and voltage were measured by an Ammeter and Voltmeter, respectively, and recorded as indicated in Table 5.3. Additionally, values of the total magnetomotive force in the circuit and current on the primary winding were also measured by the Rogowski coils to determine the induced superconducting current in the prototype coil. Considered resistance of the joints, R_j is 1.9 $\mu\Omega$ for both prototype coils, as defined in section 4.2.

Varying the voltage on autotransformer up to 6.59 V led to a magnetomotive force on primary winding up to 2388 A-t. Consequently, inducing a superconducting current on the secondary winding, i.e., into the prototype coil with four turns, producing an opposing magnetomotive force only up to 340 A-t.

Table 5.3: Tests results for a prototype coil with 4 turns.

Experimental measurements for prototype coil with 4 turns							
from Source		*from Rogowski coils*					$\mathbf{P_J = R_j \times (i_{HTS_{RMS}})^2}$
$\mathbf{U_{RMS}}$ **(V)**	$\mathbf{I_{RMS}}$ **(A)**	$\mathbf{Fmm_{A1_{RMS}}}$ **(A-t)**	$\mathbf{i_{Cu_{RMS}}}$ **(A)**	$\mathbf{Fmm_{prim_{RMS}}}$ **(A-t)**	$\mathbf{Fmm_{HTS_{RMS}}}$ **(A-t)**	$\mathbf{i_{HTS_{RMS}}}$ **(A)**	$\mathbf{P_J}$ **(mW)**
0.23	1.06	68	1.17	131	69	17.16	0.3
0.68	2.75	170	2.75	308	146	36.47	1.3
0.80	3.64	230	3.82	427	194	48.44	2.2
1.01	4.43	289	4.60	515	229	57.29	3.1
1.44	6.19	421	6.68	748	330	82.44	6.5
1.66	7.31	499	7.47	836	381	95.26	8.6
2.81	9.66	839	9.90	1109	377	94.33	8.5
3.78	12.11	1260	12.66	1417	323	80.70	6.2
4.46	14.16	1487	14.59	1634	325	81.28	6.3
5.14	16.24	1767	16.98	1902	341	85.18	6.9
5.90	18.48	2035	19.35	2167	335	83.69	6.7
6.59	20.41	2265	21.33	2388	340	85.07	6.9

Owing to the autotransformer fuse's capacity (20 A), the values of applied voltage on primary winding were below the 10 V for security precautions.

Figure 5.6 shows as an example, the characteristic waves for two distinct points of measure, i.e., magnetomotive forces on the primary winding and the induced superconducting current into the prototype coil.

In (a) for 4.60 A of applied current on primary winding, which corresponds to a magnetomotive force of 515 A-t, the superconductor follows and 57.29 A of the induced current is achieved in the prototype coil (RMS values).

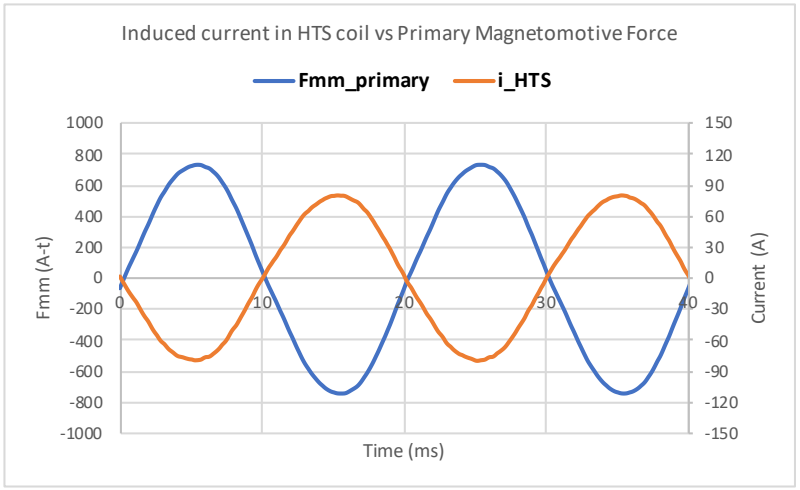

(a)

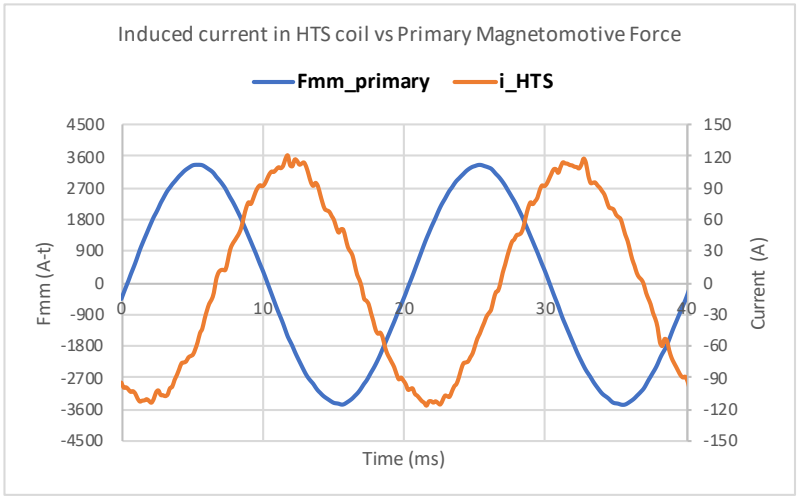

(b)

Figure 5.6: Two results for the prototype coil with four turns: (a) Magnetomotive force on the primary winding of 515 A-t and superconducting current on the secondary of 57.29 A; (b) Magnetomotive force on the primary winding of 2388 A-t and superconducting current on the secondary of 85.07 A.

In (b) for the maximum current applied of 21.33 A, corresponding to 2388 A-t of magnetomotive force on primary winding, the induced current achieve up to 85 A in the prototype coil with four turns.

The induced critical current in tape for this case is lower than the 129 A of minimum critical current, which was previously measured for the same tape used to build this prototype coil. Therefore, an additional degradation of the superconducting properties of this tape during the construction of the prototype and the tests can be appointed as one of the causes for this result.

The result of all measurements for this prototype is shown in Figure 5.7. Under large magnetomotive force is shown in (a) that the current saturates around 340 A-t, instead

of 516 A-t, if considered the minimum critical current for the tape used. This result corresponds to a maximum current in the tape of 85 A during the tests. Dissipated power in the joint is also shown for each point of measurement.

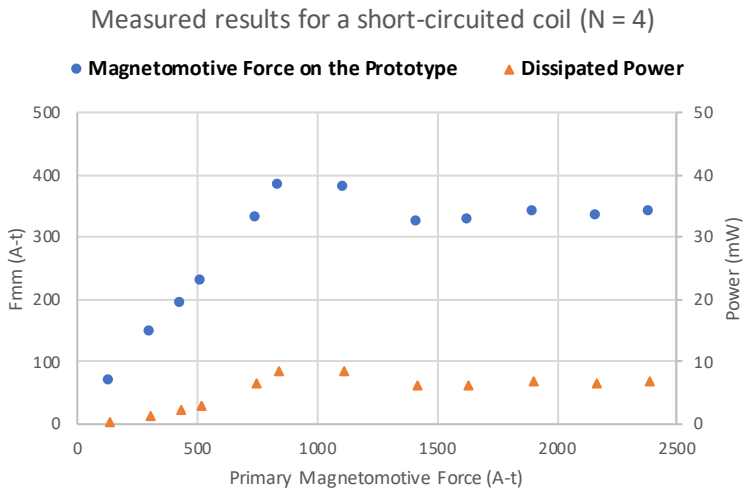

(a)

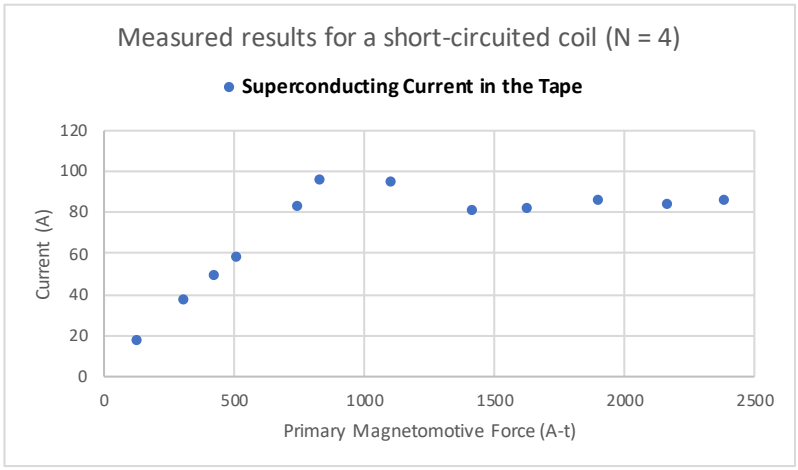

(b)

Figure 5.7: Results of the tests for the prototype coil with four turns: (a) Magnetomotive force on the prototype and maximum losses in the joint; (b) Superconducting current in tape.

In (b) is also shown the evolution of the maximum superconducting current in the tape for all the measured points.

Under large magnetomotive forces, the maximum losses in the joints are at the peak of 6.9 mW, considering the resistance of the joint for the prototype coils as determined in section 4.2.

- ***Results for the prototype coil with eight turns***

The same procedure was repeated here for the prototype coil with eight turns and Table 5.4 shows a summary of these results.

Varying the voltage on autotransformer up to 6.30 V led to a magnetomotive force on primary winding up to 2137 A-t. Consequently, inducing a superconducting current on the secondary winding producing a magnetomotive force up to 612 A-t, i.e., into the prototype coil with eight turns.

Table 5.4: Tests results for a prototype coil with 8 turns.

Experimental measurements for prototype coil with 8 turns							
from Source		*from Rogowski coils*					$\mathbf{P_J = R_j \times (i_{HTS_{RMS}})^2}$
$\mathbf{U_{RMS}}$ **(V)**	$\mathbf{I_{RMS}}$ **(A)**	$\mathbf{Fmm_{A1_{RMS}}}$ **(A-t)**	$\mathbf{i_{Cu_{RMS}}}$ **(A)**	$\mathbf{Fmm_{prim_{RMS}}}$ **(A-t)**	$\mathbf{Fmm_{HTS_{RMS}}}$ **(A-t)**	$\mathbf{i_{HTS_{RMS}}}$ **(A)**	$\mathbf{P_J}$ **(mW)**
0.68	0.95	67	1.10	123	56	7.02	0.0
0.94	2.10	126	2.10	236	111	13.89	0.2
1.60	3.60	224	3.76	421	197	24.58	0.6
2.14	6.71	410	6.73	754	377	47.08	2.1
3.13	9.17	623	9.20	1031	465	58.17	3.2
4.17	12.37	932	12.57	1408	572	71.55	4.9
4.87	14.45	1280	14.87	1666	586	73.23	5.1
5.60	16.51	1515	16.84	1886	615	76.88	5.6
6.30	18.42	1768	19.08	2137	612	76.46	5.6

The characteristic waves for one point of measure are shown in Figure 5.8, i.e., the magnetomotive force on the primary winding and the induced superconducting current into the prototype coil. An applied current of 3.76 A, which corresponds to 421 A-t on primary winding, yields 24.6 A into the prototype coil (RMS values).

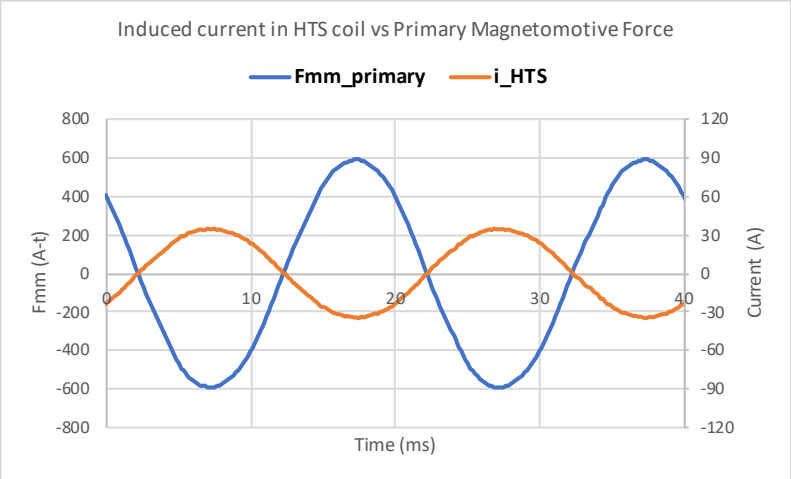

Figure 5.8: Result for one point of measure for the prototype coil with eight turns: A magnetomotive force on the primary winding of 421 A-t and superconducting current on the secondary of 24.58 A.

Figure 5.9 shows an applied current of 6.3 A, corresponding to 2131 A-t of magnetomotive force on the primary, which induces 76.5 A into the prototype coil (RMS values).

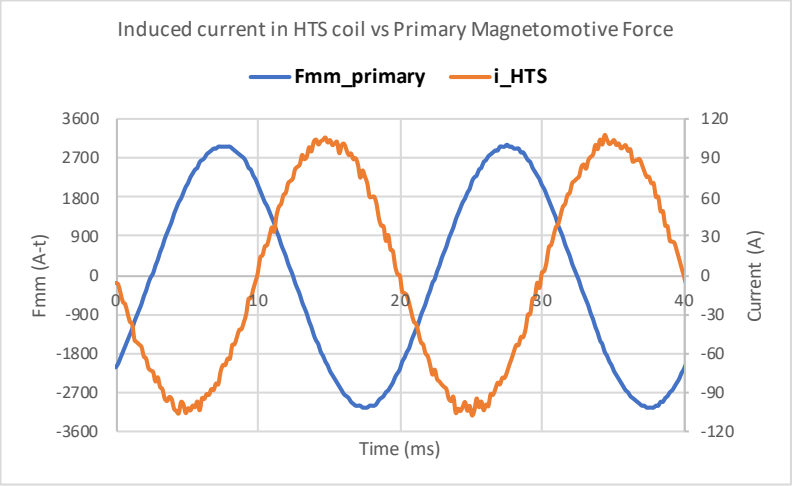

Figure 5.9: Result of the last measure for the prototype coil with eight turns: Magnetomotive force on the primary winding of 2137 A-t and superconducting current on the secondary of 76.5 A.

In this case, the maximum total induced superconducting current in the prototype coil is lower than the previous case for four turns and as shown in Figure 5.10 this prototype does not clearly saturate around 600 A-t since along the steps the induced current keeps slightly increasing even under large magnetomotive force.

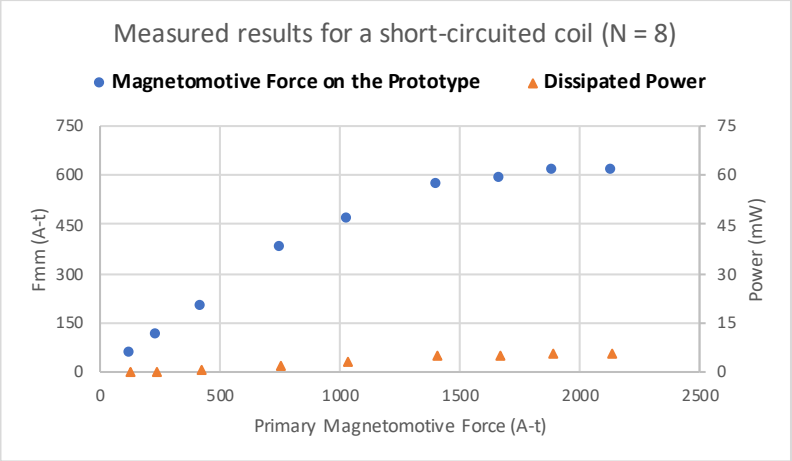

Figure 5.10: Results for the prototype coil with eight turns: Magnetomotive force on the prototype and maximum losses in the joint.

The performance of this prototype is limited due to the non-uniformity of the tape, which is related to the different values presented for different sections, as summarized in Table 3.5. This issue does not allow to assess with certainty the maximum current that this prototype coil support, besides the limitation of the current that is supported in the autotransformer and the number of turns of the primary winding.

The evolution of maximum superconducting current in the tape is shown in 5.11.

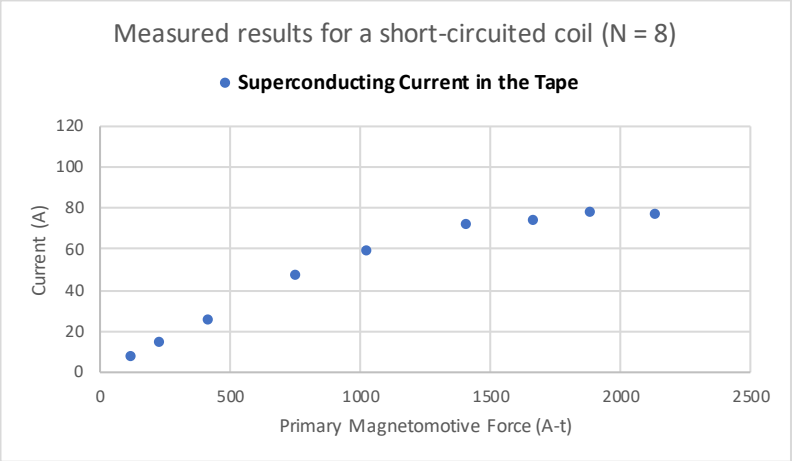

Figure 5.11: Results of the superconducting current in tape for the prototype coil with eight turns.

The expected total superconducting current in this prototype coil would be around 1333 A-t (and 666 A-t for the prototype with 4 turns), considering the result of the related work for the same type of superconducting tapes achieved in Murta-Pina et al. (2018), where the critical current and the maximum superconducting current in tape was 166.6 A.

Under large magnetomotive forces, maximum losses in the joints for the measured values are at the peak of 5.6 mW. These losses as in the previous case are below to the maximum losses measured for the prototype build in Murta-Pina et al. (2018) whose work is fully related.

5.5 Synopsis

In this chapter, was presented the specific design parameters for both prototypes coils constructed.

The process for development of both prototypes was also explained and the achieved coils presented.

The experimental procedure to measure the critical currents in the prototypes was described and the experimental results were presented and discussed.

6 | Conclusions and Future Work

In this section are presented the main conclusions obtained from the developed work. However, there are some points which were not possible to address in the present work, therefore, it should stay for future work.

6.1 Conclusions

One of the main motivations for this work was the possibility to achieve low-resistance short-circuited coils intended to be used in applications like the iSFCL in order to minimize the losses introduced by the non-superconducting joints on the secondary.

Two cutting methods for tapes were considered, namely water jet and punching. It was expected that at least one could be considered for full-scale production of the proposed architecture. However, the water jet method revealed more aggressive for the purpose despite all the advantages of the technology employed in this cut technique. The results suggest that it should be abandoned unless several modifications in the conventional machines are made.

The punching method is more mature and led to better results, aligned with those achieved when the architecture of these coils was first proposed and tested. Nevertheless, it is a restricted process making use of a patented machine specifically developed for this purpose, with access under request which suits not for easy access and large scale production.

The soldering process used to achieve the low-resistance joints was executed carefully and repeatedly, following the recommendations of the manufactures for hand-assembled splicings. However, the obtained results show that improvements could be made with a better temperature controlled device since the used oven presented some temperature variations. Real-Time Measurement of the applied pressure during the joining process would improve this method too.

Solder material applied to the joints should be as thin as possible, in the order of micrometres as recommended, which was followed. Therefore, a direct relation between

the amount of applied solder material during the process and the joints resistance was detected during the tests.

Prototype coils were achieved successful using only the tapes cut by water jet. The results obtained for the critical current on these devices was highly influenced by the cut process used on tapes, being the best values of total current in the superconducting coils achieved by the coil with four turns.

The result of the two prototypes differs when compared to a three-turn prototype previously constructed with the same superconducting material (2G HTS YBCO tapes). Either in the value of supported superconducting current, where they present about half of the expected superconducting current or in the behaviour under large magnetomotive force, where for the prototype with four turns the current saturates at a peak of 85 A, whereas for the one with eight turns the same is not clearly verified, with its value slightly increasing.

6.2 Future Work

As future work should be pointed out other methods to cut the tape such as specific lasers with less impact on the critical current density degradation, or EDM variants that should fit the purpose.

The design of a more specific device with better control of applied pressure during the joining process and the control of soldering temperature should be considered, in order to have a more homogeneous distribution of temperature for the soldering process. An important aspect which has influence in the resistance of the joints.

Other methods for making the joints, such as the diffusion, can also be tested in the future since there are reports of very good results in the literature using this type of joining process.

Future stress tests on tapes after the cut process should be considered in order to better evaluate the impact of the cut process of the tapes and it can act as an additional point to consider when choosing and enhancing the cut method.

Bibliography

Abrikosov, A. A. (2004). "Nobel Lecture: Type-II superconductors and the vortex lattice." In: *Rev. Mod. Phys.* 76.3, pp. 975–979. DOI: 10.1103/RevModPhys.76.975.

AMSC (2012). "Guidelines for Hand-Assembled Splicing of Amperium® Wire."

Badcock, R., N. Long, M. Mulholland, S. Hellmann, A. Wright, and K. Hamilton (2009). "Progress in the Manufacture of Long Length YBCO Roebel Cables." In: *IEEE Trans. Appl. Supercond.* 19.3, pp. 3244–3247. DOI: 10.1109/TASC.2009.2019065.

Bagrets, N., A. Augieri, G. Celentano, G. Tomassetti, K.-P. Weiss, and A. della Corte (2015). "Investigation of ReBCO Conductor Tape Joints for Superconducting Applications." In: *IEEE Trans. Appl. Supercond.* 25.3, pp. 1–5. DOI: 10.1109/TASC.2014.2373055.

Barth, C., G. Mondonico, and C. Senatore (2015). "Electro-mechanical properties of REBCO coated conductors from various industrial manufacturers at 77 K, self-field and 4.2 K, 19 T." In: *Supercond. Sci. Technol.* 28.4, p. 045011. DOI: 10.1088/0953-2048/28/4/045011.

Barth, C. (2013). "High Temperature Superconductor Cable Concepts for Fusion Magnets." Doctoral dissertation, p. 258. ISBN: 978-3-7315-0065-0. DOI: 10.5445/KSP/1000035747. URL: http://digbib.ubka.uni-karlsruhe.de/volltexte/1000035747.

Bednorz, J. G. and K. A. Müller (1987). "Perovskite-type oxides - The New Approach to High-Tc Superconductivity." In: *Nobel Lect.* pp. 424–457. URL: https://www.nobelprize.org/nobel{_}prizes/physics/laureates/1987/bednorz-muller-lecture.pdf.

Brittles, G. D., T. Mousavi, C. R. M. Grovenor, C. Aksoy, and S. C. Speller (2015). "Persistent current joints between technological superconductors." In: *Supercond. Sci. Technol.* 28.9, p. 093001. DOI: 10.1088/0953-2048/28/9/093001.

Buckel, W. and R. Kleiner (2004). *Superconductivity*. Ed. by W. Buckel and R. Kleiner. 2nd ed. Weinheim, Germany: Wiley-VCH Verlag GmbH, p. 464. DOI: 10.1002/9783527618507.

Can Superconductors s.r.o. (2018). *Superconducting YBCO Levitation Bulk*. URL: https://www.can-superconductors.com/levitation-bulk.html (visited on 09/02/2018).

Celentano, G. and A. Augieri (2012). "High temperature superconductivity : challenges and perspectives for electric power applications." In: *Ital. Natl. Agency New Technol. Energy Sustain. Dev.* pp. 60–71. URL: http://www.enea.it/it/seguici/pubblicazioni/pdf-eai/maggio-giugno-2012/high-temperature-superconductivity.pdf.

Chang, K. S., H. C. Jo, Y. J. Kim, M. CheolAhn, and T. K. Ko (2011). "An Experimental Study on the Joint Methods Between Double Pancake Coils Using YBCO Coated Conductors." In: *IEEE Trans. Appl. Supercond.* 21.3, pp. 3005–3008. DOI: 10.1109/TASC.2010.2092734.

Conectus.org (2018). *Supercondutivity*. URL: http://conectus.org/superconductivity/ (visited on 09/02/2018).

De Marzi, G., L. Muzzi, and P. Lee (2016). "Superconducting Wires and Cables: Materials and Processing." In: *Ref. Modul. Mater. Sci. Mater. Eng.* Vol. 4. September 2015. Elsevier, pp. 1–21. DOI: 10.1016/B978-0-12-803581-8.01917-2.

Didier, G. and J. Lévêque (2014). "Influence of fault type on the optimal location of superconducting fault current limiter in electrical power grid." In: *Int. J. Electr. Power Energy Syst.* 56, pp. 279–285. DOI: 10.1016/j.ijepes.2013.11.018.

Didier, G., C. Bonnard, T. Lubin, and J. Lévêque (2015). "Comparison between inductive and resistive SFCL in terms of current limitation and power system transient stability." In: *Electr. Power Syst. Res.* 125, pp. 150–158. DOI: 10.1016/j.epsr.2015.04.002.

Duckworth, R. C., Y. Zhang, M. J. Gouge, C. M. Rey, D. C. van der Laan, C. Clickner, and U. B. Balachandran (2010). "Voltage Distribution And Mechanical Strength In Splice Joints Made From AS-Manufactured YBCO Coated Conductors." In: *AIP Conf. Proc.* Vol. 1219, pp. 370–379. DOI: 10.1063/1.3402325. URL: http://aip.scitation.org/doi/abs/10.1063/1.3402325.

Eck, J. (2018). *Superconductors.org*. URL: http://superconductors.org (visited on 09/02/2018).

Flow International Corporation (2018). *How Waterjet Works*. URL: https://www.flowwaterjet.com/Learn/How-Waterjet-Works.aspx{\#}basics (visited on 09/02/2018).

Goldacker, W., A. Kario, S. Otten, G. Kirby, H. Bajas, J. van Nugteren, A. Ballarino, M. Bajko, L. Bottura, and G. de Rijk (2016). "Latest developments and challenges in developing Coated Conductor magnets for accelerators within EuCARD-2." In: *EuCARD-2*, p. 50. URL: https://cds.cern.ch/record/2238587/files/CERN-ACC-SLIDES-2016-0021.pdf.

Goldacker, W., F. Grilli, E. Pardo, A. Kario, S. I. Schlachter, and M. Vojenčiak (2014). "Roebel cables from REBCO coated conductors: a one-century-old concept for the superconductivity of the future." In: *Supercond. Sci. Technol.* 27.9, p. 093001. ISSN: 0953-2048. DOI: 10.1088/0953-2048/27/9/093001.

Heilmann, E.-M. (2013). "Water Jet Guided Laser Cutting of High Temperature Superconductors." In: *J. Laser Micro/Nanoengineering* 8.1, pp. 70–74. DOI: 10.2961/jlmn.2013.01.0014.

Indium-Corporation (2016). *Research Solder Kit Information*. URL: https://buy.solder.com/Low-Temperature-Pb-Free-Lead-Free-Solder-Paste-Kit/P1110{_}1040/ (visited on 09/02/2018).

Jensen Ray, P. (2015). "Structural investigation of La2-xSrxCuO4+y: Following staging as a function of temperature." Doctoral dissertation. University of Copenhagen, pp. 7–11. URL: https://doi.org/10.6084/m9.figshare.2075680.v2.

Kamerlingh Onnes, H. (1913). "Investigations into the properties of substances at low temperatures, which have led, amongst other things, to the preparation of liquid helium." In: *Nobel Lect.* pp. 306–336. URL: http://www.nobelprize.org/nobel{_}prizes/physics/laureates/1913/onnes-lecture.pdf.

Kato-Yoshioka, J., N. Sakai, S. Tajima, S. Miyata, T. Watanabe, Y. Yamada, N. Chikumoto, K. Nakao, T. Izumi, and Y. Shiohara (2006). "Low resistance joint of the YBCO coated conductor." In: *J. Phys. Conf. Ser.* 43.1, pp. 166–169. DOI: 10.1088/1742-6596/43/1/042.

Ki Sung Chang, Dong Keun Park, Seong Eun Yang, Hyun Chul Jo, Hyung Jun Kim, Yong Soo Yoon, Hyun Sung Kim, Haigun Lee, and Tae Kuk Ko (2010). "Experimental Analysis of a Splice Method Between YBCO Coated Conductors on Various Bending Diameters." In: *IEEE Trans. Appl. Supercond.* 20.3, pp. 1577–1580. DOI: 10.1109/TASC.2010.2042945.

Kim, W.-S., S. Lee, Y. Kim, J. Y. Lee, S.-H. Park, J. Lee, G.-W. Hong, J.-H. Han, and K. Choi (2015). "Persistent Current Mode of a 1-T-Class HTS Pancake Coil for NMR/MRI Applications." In: *IEEE Trans. Appl. Supercond.* 25.3, pp. 1–4. DOI: 10.1109/TASC.2014.2376593.

Krabbes, G., G. Fuchs, W.-R. Canders, H. May, and R. Palka (2006). *High Temperature Superconductor Bulk Materials*. Weinheim, FRG: Wiley-VCH Verlag GmbH & Co. KGaA, p. 314. DOI: 10.1002/3527608044.

Lehndorff, B. R. (2001). *High- Superconductors for Magnet and Energy Technology*. 1st ed. Vol. 171. Springer Tracts in Modern Physics. Berlin, Heidelberg: Springer Berlin Heidelberg, pp. XII, 212. DOI: 10.1007/3-540-40983-1.

Luiz, A. M., Z. G. Özdemir, A. Çataltepe, Ü. Onbaşlı, G.-J. Lee, and Y. Wang (2011). *Applications of High-Tc Superconductivity*. Ed. by A. Luiz. InTech, p. 272. DOI: 10.5772/2522.

MA, Y. (2004). "Second generation YBCO coated conductors: A review." In: *Chinese Sci. Bull.* 49.23, p. 2435. DOI: 10.1360/04we0094.

Maeda, H. and Y. Yanagisawa (2014). "Recent Developments in High-Temperature Superconducting Magnet Technology (Review)." In: *IEEE Trans. Appl. Supercond.* 24.3, pp. 1–12. DOI: 10.1109/TASC.2013.2287707.

Mangin, P. and R. Kahn (2017). *Superconductivity*. Cham: Springer International Publishing, p. 496. DOI: 10.1007/978-3-319-50527-5.

Murta-Pina, J., N. Vilhena, P. Arsenio, A. Pronto, and A. Alvarez (2018). "Preliminary Design and Test of Low-Resistance High Temperature Superconducting Short-Circuited Coils." In: *IEEE Trans. Appl. Supercond.* 28.4, pp. 1–5. DOI: 10.1109/TASC.2018.2820726.

Park, Y., M. Lee, H. Ann, Y. H. Choi, and H. Lee (2014). "A superconducting joint for GdBa2Cu3O7-δ-coated conductors." In: *NPG Asia Mater.* 6.5, e98–e98. ISSN: 1884-4049. DOI: 10.1038/am.2014.18.

Pina, J. M. M. (2010). "Desenho e Modelização de Sistemas de Energia Empregando Materiais Supercondutores de Alta Temperatura." Doctoral dissertation. Faculdade de Ciências e Tecnologia, Universidade Nova de Lisboa (FCT NOVA), p. 380. URL: http://hdl.handle.net/10362/5059.

Pina, J. M., M. V. Neves, A. Álvarez, and A. L. Rodrigues (2010). "High Temperature Superconducting Fault Current Limiters as Enabling Technology in Electrical Grids with Increased Distributed Generation Penetration." In: *IFIP Adv. Inf. Commun. Technol.* Vol. 314, pp. 427–434. DOI: 10.1007/978-3-642-11628-5_47.

Pronto, A. M. G. (2010). "Análise de Perdas em Sistemas de Energia que empregam Materiais Supercondutores de Alta Temperatura." Doctoral dissertation. Faculdade de Ciências e Tecnologia, Universidade Nova de Lisboa (FCT NOVA), p. 159. URL: http://hdl.handle.net/10362/5116.

Qiu, D., Z. Li, F. Gu, Z. Huang, A. Zhao, D. Hu, B. Wei, H. Huang, Z. Hong, K. Ryu, and Z. Jin (2018). "Experiment study on an inductive superconducting fault current limiter using no-insulation coils." In: *Phys. C Supercond. its Appl.* 546, pp. 1–5. DOI: 10.1016/j.physc.2017.11.011.

Qu, T., P. C. Michael, J. Voccio, J. Bascuñán, S. Hahn, and Y. Iwasa (2016). "Persistent-current switch for pancake coils of rare earth-barium-copper-oxide high-temperature superconductor: Design and test results of a double-pancake coil operated in liquid nitrogen (77–65 K) and in solid nitrogen (60–57 K)." In: *Appl. Phys. Lett.* 109.8, p. 082601. DOI: 10.1063/1.4961622.

Rose-Innes, A. C. and E. H. Rhoderick (1978). *Introduction to Superconductivity*. Ed. by P. Pergamon Press. 2nd ed. International series in solid state physics. Elsevier Inc., p. 237. ISBN: 9780080216515.

Saxena, A. K. (2010). *High-Temperature Superconductors*. Vol. 125. Springer Series in Materials Science. Berlin, Heidelberg: Springer Berlin Heidelberg, p. 218. DOI: 10.1007/978-3-642-00712-5.

Seidel, P. (2015). *Applied Superconductivity*. Ed. by P. Seidel. Vol. 1-2. Weinheim, Germany: Wiley-VCH Verlag GmbH & Co. KGaA, pp. 1–1260. DOI: 10.1002/9783527670635.

Sekitani, T, N Miura, S Ikeda, Y. Matsuda, and Y Shiohara (2004). "Upper critical field for optimally-doped YBa2Cu3O7-δ." In: *Phys. B Condens. Matter* 346-347, pp. 319–324. DOI: 10.1016/j.physb.2004.01.098.

Senatore, C., M. Alessandrini, A. Lucarelli, R. Tediosi, D. Uglietti, and Y. Iwasa (2014). "Progresses and challenges in the development of high-field solenoidal magnets based on RE123 coated conductors." In: *Supercond. Sci. Technol.* 27.10, p. 103001. DOI: 10.1088/0953-2048/27/10/103001.

Senatore, C., C. Barth, M. Bonura, M. Kulich, and G. Mondonico (2016). "Field and temperature scaling of the critical current density in commercial REBCO coated conductors." In: *Supercond. Sci. Technol.* 29.1, p. 014002. DOI: 10.1088/0953-2048/29/1/014002.

Seyeon Lee, Woo-Seok Kim, Yungil Kim, Sang Ho Park, Ji-Kwang Lee, Jin-Ho Hahn, Gye-Won Hong, Il Han Park, Chan Park, and Kyeongdal Choi (2013). "Characteristics of an HTS Pancake Coil in Persistent Current Mode Using Wind-and-Flip Winding Method." In: *IEEE Trans. Appl. Supercond.* 23.3, pp. 4601305–4601305. ISSN: 1051-8223. DOI: 10.1109/TASC.2013.2238577.

Sheng, J., M. Zhang, Y. Wang, X. Li, J. Patel, and W. Yuan (2017). "A new ring-shape high-temperature superconducting trapped-field magnet." In: *Supercond. Sci. Technol.* 30.9, p. 094002. ISSN: 0953-2048. DOI: 10.1088/1361-6668/aa7a51.

Sugano, M., S. Choi, A. Miyazoe, K. Miyamatsu, T. Ando, K. Itoh, T. Kiyoshi, H. Wada, and V. Selvamanickam (2008). "Strain Analysis of $I_{c}()$ Characteristic of YBCO Coated Conductor Measured by a Walters Spring." In: *IEEE Trans. Appl. Supercond.* 18.2, pp. 1143–1146. DOI: 10.1109/TASC.2008.922298.

SuperPower-Inc. (2013). *SuperPower® Soldering Instructions*. URL: http://www.superpower-inc.com/system/files/SP{_}Soldering+Instructions{_}2013FEC{_}v2.pdf (visited on 09/02/2018).

SuperPower-Inc. (2014). *SuperPower® 2G HTS Wire Specifications*. URL: http://www.superpower-inc.com/system/files/SP{_}2G+Wire+Spec+Sheet{_}2014{_}web{_}v1.pdf (visited on 09/02/2018).

Tinkham, M. (1996). *Introduction to Superconductivity*. 2nd ed. McGraw-Hill, Inc., p. 472. ISBN: 0-07-064878-6.

Tsuchiya, K., A. Kikuchi, A. Terashima, K. Norimoto, M. Uchida, M. Tawada, M. Masuzawa, N. Ohuchi, X. Wang, T. Takao, and S. Fujita (2017). "Critical current measurement of commercial REBCO conductors at 4.2 K." In: *Cryogenics (Guildf).* 85, pp. 1–7. DOI: 10.1016/j.cryogenics.2017.05.002.

Tsui, Y., E. Surrey, and D. Hampshire (2016). "Soldered joints—an essential component of demountable high temperature superconducting fusion magnets." In: *Supercond. Sci. Technol.* 29.7, p. 075005. DOI: 10.1088/0953-2048/29/7/075005.

Vanderbemden, P., Z. Hong, T. A. Coombs, S. Denis, M. Ausloos, J. Schwartz, I. B. Rutel, N. Hari Babu, D. A. Cardwell, and A. M. Campbell (2007). "Behavior of bulk high-temperature superconductors of finite thickness subjected to crossed magnetic fields: Experiment and model." In: *Phys. Rev. B* 75.17, p. 174515. DOI: 10.1103/PhysRevB.75.174515.

Woo-Seok Kim, Chan Park, Sang Ho Park, Jikwang Lee, Jung-Bin Song, Haigun Lee, Hee-Gyoun Lee, Gye-Won Hong, and Kyeongdal Choi (2009). "Magnetic Field Stability of a Small YBCO Magnet in Persistent Current Mode." In: *IEEE Trans. Appl. Supercond.* 19.3, pp. 2194–2197. ISSN: 1051-8223. DOI: 10.1109/TASC.2009.2018750.